

Sea Surface Water Motion off Chile Latitudes
18°S-40°S, Revealed from Satellite Images of
Chlorophyll and Temperature Distribution

by

Felix R. Espinoza

A THESIS

submitted to

Oregon State University
(School of Oceanography MRM)

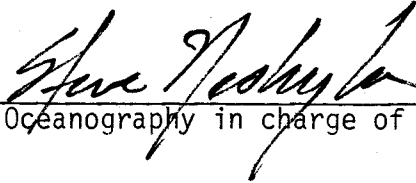
in partial fulfillment of
the requirements for the
degree of

Master of Science

Completed August 26, 1983

Commencement June 1984

APPROVED:



Professor of Oceanography in charge of major

Acting Dean of College of Oceanography

Dean of Graduate School

Date thesis is presented August 26, 1983

Typed by Donna Lee Norvell-Race for Felix R. Espinoza

❖ DEDICATED TO

My dear wife, Karin

My parents and sisters

My country

My friend, Geoff


AN ABSTRACT OF THE THESIS OF

Felix R. Espinoza for the degree of Master of Science

in Oceanography presented on August 26, 1983

Title: Sea Surface Water Motion off Chile Latitudes 18°S-40°S,
Revealed from Satellite Images of Chlorophyll and
Temperature Distribution.

Abstract approved:


Dr. Steve Neshyba

The mesoscale sea-surface circulation pattern within 400 km off Chile and between 18°S and 40°S latitude is described using chlorophyll and temperature images from the Coastal Zone Color Scanner NIMBUS-7 satellite. The data base is a set of four mosaics developed from band-3 (550 nm) images taken on June 4 and September 16, 1979 and January 14 and April 7, 1980, supplemented with one mosaic of sea-surface temperature distribution for the September mosaic, orbit 4526.

Coastal eddies, upwelling zones and zones of onshore-offshore transport are clearly distinguished because a zone of low-pigment concentration water generally separates the highly pigmented near-shore upwelling zones from oceanic waters with pigment concentration in mid-range. The cause of the low-pigment water adjacent to upwelling zones is not known, but the absence of temperature

differences between upwelled and low-pigmented water suggest a biological cause.

Onshore jets of oceanic waters are traced from distances up to 300 km offshore to within, in places, a few tens of kilometers of the shoreline; width of the jets is of the order of 60 km. In general, these onshore jets are separated by plumes of nearshore surface water moving seaward, with plumes width on the order of 40 km also extending as far as 400 km offshore. Large eddies form off the leading edges of both onshore and offshore plumes, giving rise to a formation called a "hammerhead" structure. Onshore jets are consistent with the result of Inostroza (1972) which documents intrusions of warm oceanic surface waters as semi-stationary features off Coquimbo (30°S) and off Talcahuano (37°S).

Lack of wind data for 1979-80 prevents a direct correlation of onshore-offshore plumes with regional wind stress data. Low level wind charts for the 1979-80 period are too coarse in resolution to yield correlations. However, stick diagrams were prepared from coastal wind station data for 1977. Both time and space variations in surface winds could be responsible for the patterns revealed in chlorophyll images.

The existence of persistent but probably episodic onshore-offshore transport of surface waters to such large distances offshore have not been reported previously for Chilean waters. These must certainly impact directly the patterns of migrations of populations of major fishery resources such as the Jack Mackerel (Trachurus murphyi, common name Jurel, species.

TABLE OF CONTENTS

	<u>Page</u>
I. INTRODUCTION	1
II. BACKGROUND	5
Water Masses.	5
Subtropical Surface Water.	5
Subantarctic Water	5
Equatorial Subsurface Water.	7
Antarctic Intermediate Water	7
Pacific Deep Water	8
Circulation	8
The Humboldt Current	8
The Peru Countercurrent.	10
The Peru Undercurrent.	10
Upwelling	11
Large-scale Eddy Structure.	13
III. MATERIALS AND METHODS.	16
Satellite Images.	16
Meterological Charts.	21
Source	21
Interpretation	22
Coastal Wind Data	23
IV. DESCRIPTIVE ANALYSIS	29
Winter Season	29
Upwelling.	29
Low Pigment Concentration Zones.	31
Coastal Intrusions of Oceanic Waters	35
Autumn Season	37
Upwelling.	37
Coastal Intrusions of Oceanic Waters	41
Summer Season	42
Upwelling.	42
Low Pigment Concentration Zones.	46
Onshore-Offshore Surface Motion.	48

	<u>Page</u>
End of the Autumn Season	51
Upwelling	51
Low Pigment Concentration Zones	55
Onshore Intrusion of Oceanic Waters	55
Temperature Mosaic	56
V. DISCUSSION AND CONCLUSIONS.	61
VI. APPLICATIONS OF CZCS NIMBUS-7 REMOTE SENSED DATA IN CHILE	80
BIBLIOGRAPHY.	85
APPENDICES	
A Fortran Listing of Filter Subroutine Used with the Coastal Wind Time Series	89
B Fortran Listing of Plot Subroutine Used to Make the Wind Stick Diagrams . . .	92
C Meteorological Charts.	99

LIST OF FIGURES

<u>Figure</u>		<u>Page</u>
1	Area of study along the coast of Chile	6
2	Origin of the Humboldt System from the division of the West Wind Drift (40°S) (from Silva and Neshyba, 1977)	9
3	Potential acceleration map showing an eddy structure off Chile at 21°S (from Silva and Sievers, 1981)	15
4	Mosaic of chlorophyll images along the coast of Chile. Orbit N 4526. September 16, 1979. Band 3 (550 nm)	30
5	Small mosaic of chlorophyll images along the coast of southern Chile. Orbit N 2232. April 3, 1979. Band 1/Band 3 ratio (443/550 nm)	33
6	Mosaic of chlorophyll images along the coast of Chile. Orbit N 7345. April 7, 1980. Band 3 (550 nm)	38
7	Mosaic of chlorophyll images along the coast of Chile. Orbit N 6184. January 14, 1980. Band 3 (550 nm)	44
8	Mosaic of chlorophyll images along the coast of Chile. Orbit N 6184. January 14, 1980. Band 1/Band 3 ratio (443/550 nm)	50
9	Hammer Head structure and associated eddy processes, revealed in the chlorophyll mosaic for January 14, 1980. Orbit N 6184. Band 1/Band 3 ratio (443/550 nm)	52
10	Mosaic of temperature images along the coast of Chile. Orbit N 3089. June 4, 1979. Band 3 (550 nm)	53
11	Mosaic of temperature images along the coast of Chile. Orbit N 4526. September 16, 1979. Band 6 (10.5-12.5 μ m)	57

<u>Figure</u>		<u>Page</u>
12	Average sea surface temperature off the coast of Chile. Spring season (from Inostroza, 1972)	70
13	Average 50 m depth temperature off the coast of Chile during Spring (from Inostroza, 1972)	71
14	Average 100 m depth temperature off the coast of Chile, during Spring (from Inostroza, 1972)	72
15	Wind time series for six stations along the coast of Chile. Nine months (January-September) 1977. Diurnal frequencies have been filtered	76
16	Chart of sea-surface temperature data off the coast of Chile. It shows the density of the data concentrated along 40°S latitude and 200 miles offshore, which reflects the concentration of fishing boats catching Jurel, Jack Mackerel (<u>Trachurus murphyi</u>)	83

LIST OF TABLES

<u>Table</u>		<u>Page</u>
I	Orbit information of the chlorophyll images used to form along shore mosaics.	20
II	Wind speed in knots and wind direction relative to the geographic north. (May 29 to June 4, 1979)	24
III	Wind speed in knots and wind direction relative to the geographic north. (September 9 to September 16, 1979)	25
IV	Wind speed in knots and wind direction relative to the geographic north. (January 7 to January 14, 1980)	26
V	Wind speed in knots and wind direction relative to the geographic north. (April 1 to April 7, 1980)	27
VI	Wind station location along the coast of Chile.	28

Sea Surface Water Motion off Chile Latitudes
18°S-40°S, Revealed from Satellite Images of
Chlorophyll and Temperature Distribution

I. INTRODUCTION

The general circulation pattern of sea surface waters off Chile and the current system along the west coast of South America, in particular, has been surveyed for many years using hydrographic research vessels. These studies have increased in number during the last decade, principally in the El Niño Phenomenon studies carried out by the Hydrographic Institute of the Chilean Navy and by the Instituto the Fomento Pesquero,^{*} but also in investigations made by Universities. The region is generally characterized by a mixture of several water masses and by a general circulation pattern dominated by the Humboldt Current system.

The general circulation pattern is mainly governed by the field of wind stress generated by the Southeast Pacific Anticyclonic cell. The complexity of the pattern and the limited data available from ship cruises have been the limiting factors in circulation studies. There are no comprehensive data which are closely spaced samples, synoptic and cover the entire coastal and near-coastal waters along the coast of Chile prior to the satellite images used in this work. Remote sensed data from the Coastal Zone Color Scanner (CZCS) in

^{*} National Institution of Research in charge of promoting and improving the fishery industry of Chile.

the NIMBUS-7 has been used to complement shipboard data in studies of smaller scale features in the California Current (Smith et al., 1982; Eppley and Baker, 1982; Smith and Baker, 1982) and also in the Atlantic Ocean (Gordon et al., 1983). These efforts and the analyses reported in this paper show that remote sensing data provide a very useful complementary tool to study the more complex features in general sea surface circulation patterns.

The objective of this work is to provide a detailed description of the sea surface circulation structures and associated processes revealed in chlorophyll-concentration images and temperature-distribution images from the NIMBUS-7 satellite, CZCS. The images were processed in the Visibility Laboratory at Scripps Institution of Oceanography. Raw images are recorded in the NIMBUS-7 CZCS as a series of six co-registered images, each from preset spectral bands scanned by the sensor. Each image is recorded in a matrix of resolution elements of size 940 x 1960 (pixels). Our mosaics formed from two bands and temperature images contain 10 million data points.

This very large data base is unprecedented for the Chilean ocean. The ability to "see" structure patterns in surface waters never seen before has placed a new burden upon descriptive oceanography in that descriptions must also be detailed (and somewhat lengthy, as the reader will come to appreciate). We have chosen to describe surface patterns in detail.

Because of the complexity of the features revealed in the

images, it is necessary to establish a nomenclature related with the description of the sea surface structure.

The word "developed" is used to refer to the degree of development of the feature in time and space, neither of these implying the other. The word "defined" establishes how well-revealed is the feature in terms of the range of pigmentation of the waters involved within the structure. The word "clear" is used to state the degree of resolution of the image itself. Besides those three words there are some terms used to refer to the features or structures themselves.

The term "plume" is referred to offshore extensions of coastal or near-coastal waters. The term "intrusion" or "jet" refers to onshore surface flows of oceanic waters; in a few cases it is also used to describe coastal waters intruding oceanic regions. Other terms like LPCZ, upwelling zones, large-scale eddy structures, coastal eddies, transition zones, etc. are applied within the text and are explained in the appropriate section.

This paper presents, first, a general description of the sea surface circulation pattern of the study area using previous studies based upon hydrographic data. A Materials and Methods section precedes a detailed description of the sea surface processes within the area of interest, using five processed mosaics (four of chlorophyll concentration and one of temperature distribution) derived from scanning radiometers on the NIMBUS-7 satellite. Finally, an analysis and discussion of the information revealed from the images

together with wind-vector charts for six-day periods preceding each mosaic is presented. In the discussion, nine months time series of measured wind data from six stations along the Chilean coast are analyzed. They correspond to the period January-September, 1977, and were the only wind data available until now.

II. BACKGROUND

The study area extends from 18.5°S to 39.5°S along the coast of Chile and from the coast to an average of 400 km offshore (Figure 1). One of the first studies describing the oceanic conditions within that area was made by Gunther (1936), who presented a general study of the circulation off Chile and Perú. His work, together with that of others, forms a background base for a general description of the oceanographic conditions within the area of interest. Wyrтки, Sievers, Neshyba, and Silva are among those authors who have made significant contributions.

Water Masses

Five water masses are reported to be present within the study area:

1. Subtropical Surface Water (SSW), as defined by Wyrтки (1965), has a relatively high salinity ($35^0/00$), high temperature (19°C - 24°C) and low sigma-t (25.00); it is located just below the mixed layer. This water mass has been detected as far as $32^{\circ}59'S$ latitude (Silva and Sievers, 1981). Silva and Konow (1975) reported the SSW extending to 22°S latitude southward and between the surface and 60 m depth.
2. Subantarctic Water (SAW), which originates at the boundary of the polar front, has a comparatively low salinity (34.3 - $34.7^0/00$), low temperature (12° - 16°C) and a sigma-t of 26.00 at the core.

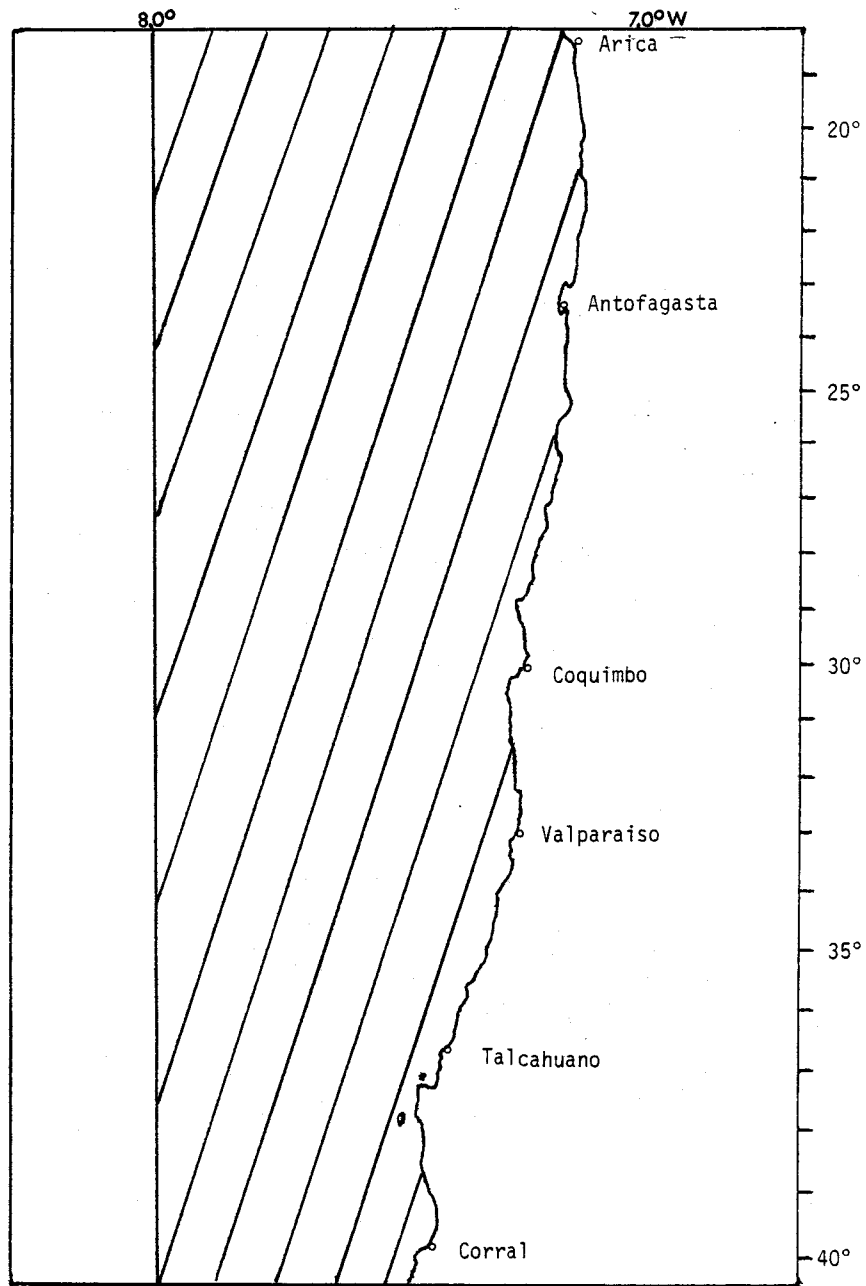


FIGURE 1. Area of study along the coast off Chile.

It is located at the subsurface layer and it has been reported extending further northward to 18°28'S (Silva and Sievers, 1981). Thickness for SAW is 160 m between 32°59'S and 26°22'S latitude and diminishes to about 100 m farther northward below the SSW. In general, the SAW varies in thickness between 250 m and 400 m, being thicker northward along the coast with its deepest limit at about 500 m (Silva and Sievers, 1981).

3. Equatorial Subsurface Water (ESSW) appears to be responsible for the presence of warm, saline, low oxygen content waters intruding from the north. It has a temperature of (13°C), relatively high salinity (34.75⁰/oo) and low oxygen content (0.25 ml/l). The intrusion covers a wide area between Arica (18.5°S) and Iquique (20.1°S) and it becomes narrower along the coast as far as it moves southward. The southernmost extension of this water mass has been reported to be as far as 37°S (Silva and Konow, 1975). However, Silva and Neshyba (1979) stated that the characteristic of ESSW can be found even farther south. They show the ESSW extending to about 48°S; further south this water mass disappears due to mixing with Subantarctic Water and Antarctic Intermediate Water.
4. Antarctic Intermediate Water (AIW), formed at the Antarctic Convergence region, is found at deeper levels within the study area. It has temperatures less than 7°C, a sigma-t of 37.20, salinity of 34.5⁰/oo and low values of dissolved oxygen. Its core is found between 640 m and 720 m depth within the study

area (Silva and Sievers, 1981). Apparently this water mass does not become part of the near-surface layers; therefore, it does not contribute to the radiance levels measured by remote sensors.

5. Pacific Deep Water (PDW), which is located below the AIW, has very low temperature, less than 4°C, and salinities of about 34.5⁰/oo. This water mass is not present within near-surface layers.

Circulation

Surface flow along the coast of Chile is predominantly equatorward and it is mainly dominated by the Humboldt Current system. It originates from the division of the Antarctic Circumpolar Current or West Wind Drift between 40°-45°S, as described by Silva and Neshyba (1977). One branch continues eastward as the Antarctic Circumpolar Current or Corriente del Cabo de Hornos, reaching the South Atlantic after crossing the Soctia Ridge through the Drake Passage. A second branch turns to the north, flowing along the coast of Chile as the Humboldt Current or Chile-Perú Current (Figure 2). This equatorward surface flow is partially sustained by wind blowing from the southwest, generated by the semi-stationary high-pressure cell of the eastern South Pacific.

The Humboldt Current, as reported by Robles et al. (1974) has velocities between 0.1 and 0.3 knots and transport values of 10 to 15 Sv between 0-200 m and 200-400 m depth. It is divided into two branches just north of 40°S latitude, the coastal and the oceanic

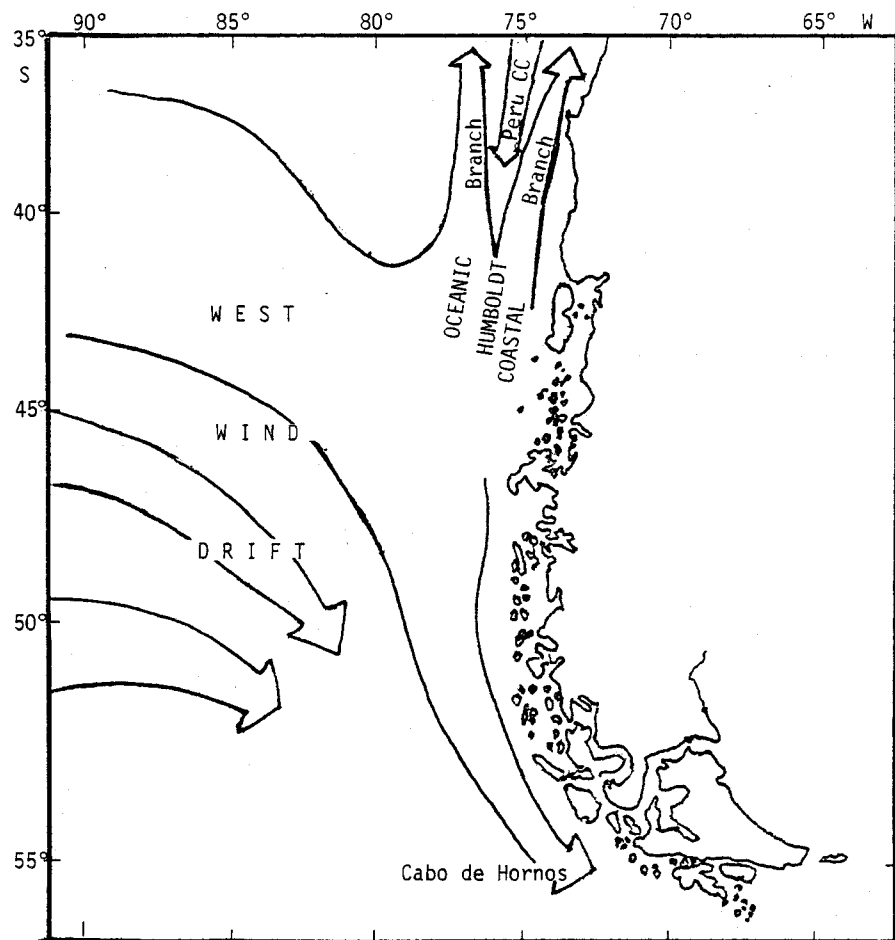


FIGURE 2. Origin of the Humboldt System from the division of the West Wind Drift (40°S) (from Silva and Neshyba, 1977).

branches, both flowing parallel to the shoreline. The coastal branch flows between near coastal areas and approximately 150 km offshore, with a general direction northward to about 20°S (Robles et al., 1974). At that latitude it diverges to the west and then to the north following the topography of the Perú coastline as the Perú-Chile Current. This equatorward flow is narrow along the coast of Perú. The oceanic branch apparently is wider than the coastal branch but it does not appear as well-defined in the literature as the coastal branch. As a general statement, it flows northward between 250 and 500 km from 40°S to about 21°S latitude. At this latitude it turns to the west as part of the Subtropical Anticyclonic Gyre, as described by Neshyba and Mendez (1975) during winter conditions.

The Perú Countercurrent, as described by several authors (Sievers and Silva, 1975; Wyrтки, 1967, 1966 and 1963; Gunther, 1936; and others), is a surface flow southward originating off Perú and extending southward to about 35°-40°S latitude between the coastal and oceanic branches of the Humboldt Current. Silva and Sievers (1981) detected a surface flow centered along 72°W with low velocities at surface which increase with depth. They stated that the core of this southward flow is associated with the Equatorial Subsurface Water, concluding that this current should be part of the surface outcrop of a southward subsurface flow, the Perú Undercurrent.

The Perú Undercurrent, as described by several authors

(Wooster and Gilmartin, 1961; Brandhorst, 1971; Sievers and Silva, 1975; Robles et al., 1976; Silva and Neshyba, 1979; Silva and Sievers, 1981; and others), is a subsurface poleward flow that transports water of high salinity, high nutrient content, and low oxygen content along the west coast of South America. It flows close to the coast and extends as far as 48°S latitude (Silva and Neshyba, 1979). Silva and Neshyba also stated that from 27°S down to 48°S the flow appears to be centered closer to the coast than from 27°S northward. The volume transports reported for this subsurface current are $4 \times 10^6 \text{ m}^3/\text{sec}$ off Antofagasta (23.3°S) and $2.4 \times 10^6 \text{ m}^3/\text{sec}$ off Valparaiso (33°S) (Silva and Sievers, 1981). This poleward flow is associated with the ESSW, which has its core generally located between 160 and 140-c1 ton^{-4} isanosteric surfaces, as reported by Silva and Neshyba (1979). Silva and Sievers (1981) reported velocities for this current between 9 cm/sec and 20 cm/sec at the core.

Upwelling

The distribution of water masses gives important clues about the origin of upwelling water. The coastal branch of the Humboldt Current, topped by a thin layer of Subtropical Surface Water, brings Subantarctic Water to about 15°S latitude. Below this, a poleward flow of Equatorial Subsurface Water occurs, concentrated in the Perú Undercurrent along the coast and in the Perú Counter-current further offshore at the surface. Wyrтки (1963) characterized

Equatorial Subsurface Water by the temperature-salinity line from $17^{\circ}\text{C}-35.2^{\circ}/\text{oo}$. The almost isohaline water above 100 m, present from $15^{\circ}40'\text{S}$ southward, was attributed by Wyrтки to Equatorial Subsurface Water upwelled near the coast and transported offshore by Ekman drift.

Wyrтки (1963, 1966) concludes that upwelling near the coast is restricted to depths of less than 100 m. South of 15°S latitude, the upwelled waters are supplied by Subantarctic Water (relative low salinity) flowing northward with the Humboldt Current. However, there is other evidence that indicates that the Equatorial Subsurface Water (relatively high salinity) which flows southward with the Perú Countercurrent, also supplies water for upwelling processes along the coast of northern Chile, perhaps as far as 25°S latitude (Basten, 1981).

Basten also reported that the Mejillones Peninsula (23°S) may intensify the upwelling within that area. This appears to be important in the sense of possible explanations for some offshore extension of upwelled waters located around headlands, which have been reported in some later studies using satellite images (Breaker and Guilliland, 1981; Espinoza et al., 1983).

Upwelling has been detected during all seasons along the coast of Northern Chile ($18^{\circ}\text{S}-26^{\circ}\text{S}$) (Basten, 1981). It is strongest during the austral spring and summer when the south and southwest winds are strongest (September-March). In general, the overlap of latitudes at which different water masses supply the water for upwelling

is probably a result of observations at different seasons of time lapses. Nevertheless, there is evidence of alongshore change within the nearshore biological regime from Antofagasta (23°S) southward, perhaps as far as 29°S , as reported by Uribe and Neshyba (1983).

Large-scale Eddy Structures

As stated earlier, circulation patterns of seasurface waters off Chile have been reported as mainly governed by the Humboldt Current system and the Perú Current system and to some extent by the wind stress pattern generated by the semi-stationary anticyclonic cell of the South Pacific. These general meso-scale descriptions, using small-scale measurements, apparently do not show strong evidences of different kinds of structures, like large-scale eddies, as major events within the near-coastal seasurface circulation patterns. However, there are some evidences of large-scale eddies as permanent features of the seasurface off northern Chile, reported by Silva and Sievers (1981). They also pointed out that this feature has been reported by Wyrтки (1963), Inostroza (1973) and Robles et al. (1976).

Silva and Sievers (1981) detected an anticyclonic eddy structure located at 21°S latitude and about 130 km offshore (Figure 3). They also stated that the eddy was evident even at subsurface levels. Apparently this eddy would be a result of an interaction of warm and colder waters mixing, resulting in a greater dynamic height within the area. They finally pointed out that the

information available for their work was not sufficient to give a better description and a possible explanation for the presence of that phenomenon.

III. MATERIALS AND METHODS

Satellite Images

Biological constituents appear to play a dominant role in the physical processes which relate the upwelling radiance emitted from the seasurface to the constituents of the water. The most important of these constituents appears to be the phytoplankton. These small organisms contain chlorophyll, which is the dominant photosynthetic pigment (Hovis et al., 1980). This pigment absorbs very strongly in the spectral window scanned by radiometers. Therefore, the increase in phytoplankton concentration (chlorophyll-a) has the effect of changing the color of the seawater from dark blue to green hues. This phenomenon can be clearly distinguished within chlorophyll images showing seasurface pigment concentration. In that way, meso-scale circulation patterns of near-surface waters (0-10 m) can be detected by image analysis.

Algorithms relating remote-sensed optical measurements to microbiological activity and associated physical processes within seasurface waters have been described by several authors. Hovis et al. (1980), Gordon et al. (1980), Austin and Petzold (1981), and Smith and Wilson (1981) have provided an algorithm which estimates the upwelling subsurface radiance from the total radiance received by the satellite sensor on NIMBUS-7, The Coastal Zone Color Scanner.

As described by Gordon et al. (1983), the Coastal Zone Color Scanner (CZCS) on NIMBUS-7 is a scanning radiometer that can obtain

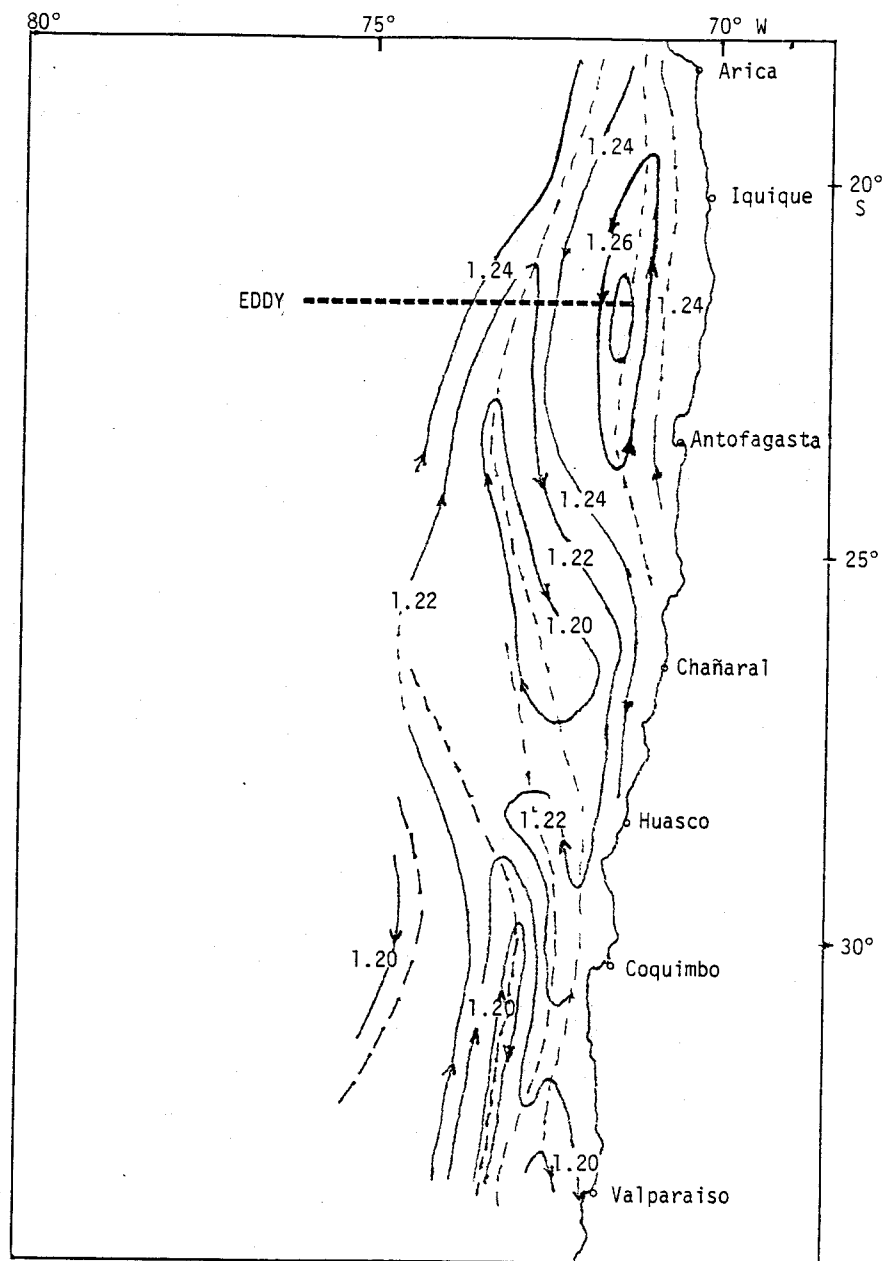


FIGURE 3. Acceleration at $\sigma_{\theta} = 26.09$ surface. Eddy structure at 21°S (from Silva and Sievers, 1981).

a view of the seasurface within six co-registered spectral bands. The first five of these bands are in the visible spectrum (443, 520, 550, 670 and 750 nm). The sixth band is a thermal infrared band (10.5-12.5 μm). The sensor has an active scan of 78° centered at the nadir and a field of view of 0.0495° , which produces a ground resolution of 825 m at the nadir from a nominal height of 955 km. The sensor is equipped for tilting the scan plane $\pm 20^\circ$ from the nadir in 2° increments along the satellite path to minimize the influence of direct sun glint, which contributes to the sensor radiance from photons which are specularly reflected from the seasurface. The satellite is in a sun-synchronous orbit with the ascending node near local noon.

Four processed mosaics constructed from chlorophyll images and one constructed from thermal images were selected from a total of fifty-two images processed in the Visibility Laboratory at the Scripps Institution of Oceanography. The images are recorded in a matrix of resolution elements (pixels) of size 900×1960 pixels. Each of those pixels represent a seasurface area of about $6.4 \times 10^5 \text{m}^2$.

The chlorophyll images were processed within the spectrum windows centered at 443 nanometers (band-1) and 550 nanometers (band-3). Chlorophyll images were also processed in the ratio of band-1 and band-3 radiances which are currently used to estimate total values of chlorophyll concentration (phytoplankton pigment

concentration). Six of the images were processed for radiance in the thermal band, centered at 10.5-12.5 μm (band-6). These thermal images correspond to the mosaic taken at the end of the winter season, September 16, 1979, and they show the seasurface temperature distribution of the area covered.

Polaroid prints and 35 mm slides were taken of each processed image using black-and-white high-resolution film. The four mosaics used here were formed using prints of images representing the back-scattered radiance centered at band-3 (550 nm). It is assumed, for the present work, that accessory phytoplankton pigments co-vary with chlorophyll-a and that the remotely sensed signal is related to the "chlorophyll-like" pigment concentration, which is the sum of chlorophyll-a and Phaeopigment-a; the latter possesses nearly the same absorption spectrum as chlorophyll-a, therefore it cannot be separated from chlorophyll-a when the CZCS bands are used (Smith and Baker, 1982). Hence, the terms chlorophyll concentration and pigment concentration are used within this paper to represent all of the chlorophyll-like pigments that can be detected by the satellite sensor. Band-3 images were chosen to form the chlorophyll mosaics because they display most clearly the different structures that dominate the seasurface circulation pattern.

Due to the difficulties in obtaining images sufficiently free of clouds, it was not possible to obtain the necessary images to form mosaics covering the same area at all seasons within a one-year time-period. The selected mosaics were taken June 4,

1979, September 16, 1979, January 14, 1980 and April 7, 1980. Orbit numbers and detailed characteristics of each of the images composing the mosaics are shown in Table 1.

Each mosaic represents a specific time-lapse instantaneous view of the area that it covers. Within the chlorophyll mosaics, the very light areas represent the higher pigment concentration, the darker areas denote relatively low pigment concentration. The very black areas of these images represent either clouds or land; the coastline of Chile is located at the right side of the mosaic, which is oriented south-north (bottom to top). The mosaic showing sea-surface temperature distribution also displays light and dark areas. In this case, the light areas represent colder waters while the dark areas represent warmer waters. Clouds and land are also represented by the very black areas, as in the case of chlorophyll images.

Chlorophyll images also display mid-range pigment concentration, as well as thermal ones do, but with less definition (seen in the pictures by the gradation from white through gray to black). This might be important in the determination of coastal, near-coastal and oceanic waters based upon the physical processes which transport water, within surface layers, with different pigmentation depending on source zones. Actual values of chlorophyll concentration are discussed by Uribe and Neshyba (1983) where the same study area is presented in terms of the ratio of band-1 and band-3 radiances, in some cases using similar satellite orbits.

TABLE I. Orbit information of the chlorophyll images used to form along shore mosaics.

Orbit N°	Date MM DD YY	Time ^a HHMMSS	Scene N°	Matrix Origin		Matrix Size Pixels N°	Band-3 ^b Max-Rd	Area Covered Latitude
				X	Y			
3089	06 04 79	172041	1	1075	080	512 x 320	3.35	31°00'00"S
3089	06 04 79	172041	2	900	400	512 x 400	3.30	to
3089	06 04 79	172252	3	1200	600	512 x 370	3.10	39°00'00"S
4526	09 16 79	170426	1	400	001	512 x 512	7.80	28°00'00"S
4526	09 16 79	170626	2	890	170	512 x 512	6.60	
4526	09 16 79	170626	3	388	170	512 x 512	6.80	
4526	09 16 79	170626	4	688	670	512 x 300	6.90	to
4526	09 16 79	170626	5	176	670	512 x 300	5.50	
4526	09 16 79	170805	6	908	620	512 x 300	6.50	39°20'00"S
6184	01 14 80	164556	1	050	001	512 x 512	7.50	20°00'00"S
6184	01 14 80	164756	2	510	001	512 x 512	5.60	
6184	01 14 80	164756	3	100	001	420 x 250	7.30	
6184	01 14 80	164756	4	320	500	512 x 470	3.10	to
6184	01 14 80	164756	5	001	458	330 x 512	6.95	
6184	01 14 80	164956	6	730	530	512 x 440	4.54	
6184	01 14 80	164956	7	220	530	512 x 440	5.60	34°00'00"S
7345	04 07 80	170915	1	960	001	512 x 512	7.84	18°00'00"S
7345	04 07 80	171115	2	1400	001	512 x 512	5.69	
7345	04 07 80	171115	3	1240	500	512 x 470	8.47	
7345	04 07 80	171115	4	1150	001	250 x 470	4.28	to
7345	04 07 80	171115	5	1040	500	200 x 470	8.28	
7345	04 07 80	171315	6	1454	500	512 x 470	8.28	
7345	04 07 80	171315	7	945	500	512 x 470	6.09	33°00'00"S

^aThe time is referred to GMT.

^bThe maximum values for radiance in band-3 are absolute values of the images without filtering.

Meteorological Charts

Source

The National Environmental Satellite Service (NEES) of the National Office of Atmospheric Administration (NOAA) infers low-level winds from low-cloud motion vectors two times a day. Low-cloud motion vectors are traced between successive infrared images taken by the Geostationary Operational Environmental Satellite (GEOS). These low-level wind charts following low-cloud stream lines provide useful information to estimate sea-surface wind stress patterns.

The vectors are determined over a 2.5° latitude by 2.5° longitude staggered grid. They are representative of the mesoscale patterns of convective clouds which are moving due to the wind force at levels between 850 mb and 900 mb, between 100 m and 1500 m altitude (Enfield, 1981).

Four series of low-level wind charts, each one covering a six-day period before the date of each of the chlorophyll mosaics analyzed, were generously provided by Dr. William Quinn, professor at Oregon State University. The series include two charts per day taken at 0000 GMT and 1200 GMT, respectively. The area covered by the wind charts extends from the equator to 55°S latitude and from the west coast of South America to 170°W longitude. Charts are included in Appendix C.

Anticyclonic circulation cells are indicated by capital letter "A" and cyclonic circulation cells area are indicated by capital

letter "C". Small arrows represent wind vectors. Lines at their tails represent wind speed at the specific location of the vector. The smaller speed lines represent five knots and the large ones ten knots, the total speed is the sum of all the small lines of each vector.

Interpretation

As stated earlier, these low-level wind charts can be used to estimate the general sea-level wind stress pattern. However, there are some factors that can diminish the representativeness of these cloud-level winds as surface winds. Three of these factors were analyzed in some detail by Enfield (1981): (1) The wind shear contamination of cloud-motion vectors, estimated as the natural variability in convective cloud heights; (2) the natural variability in the boundary-layer profile between the two levels (cloud-level and sea-level), which are in part due to possible changes in atmospheric stability; and (3) the limitation in the accuracy of estimation procedures. He stated that all of these factors are influenced by the unpredictability of convective atmospheric motion at subsynoptic time and space scales and that, therefore, better representativeness can be expected at lower frequencies than at higher ones. With that information, and taking into account that wind speed and direction over the southeastern Pacific do not show great variability for the time lapses analyzed, no adjustments have been made to the boundary layer winds used here.

The mean zonal and meridional flow of the wind components

over the southeast Pacific are estimated to be good approximations for inferring surface patterns of wind stress within the study areas covered, especially to see, in a general sense, if wind pattern during the one-week period before the satellite images were taken shows a correspondence with oceanic motions derived from the chlorophyll images.

The main information derived from stream lines and wind vectors are summarized in Tables 2, 3, 4, and 5, each one corresponding to a one-week period preceding each of the chlorophyll image mosaic dates. The tables include the main location of the cells, daily average wind speed and direction and probable convergence and divergence zones.

Coastal Wind Data

Time series of coastal wind for six stations along the coast of Chile are included to investigate the possible existence of short-time non-seasonal variability of the coastal wind field within specific zones in the study area. The length of the time series is nine months; data for spring season are missing. Unfortunately, our data are for 1977; 1979 data are not yet available.

Locations of the stations are shown in Table 6; wind speed (in knots) and wind direction are referred to geographic north. Each time series was broken into north and east components.

Stick diagrams for each of the stations were made using a subroutine plot available at the Oregon State University Computer Center. (The diagrams are shown in Figure 12, in the Discussion section.)

TABLE II. Wind speed in knots and wind direction relative to the geographic north.*

Date MM DD YY	Type of Cell	Center of the Cell		Nearshore Wind Speed Direction
		Latitude	Longitude	
05 29 79	A ^α	32°00'00"S	84°00'00"W	10 kt NE
05 30 79	A	32°00'00"S	84°00'00"W	5 kt N NE
05 31 79	A	27°30'00"S	113°00'00"W	5 kt E N
06 01 79	A	27°00'00"S	125°00'00"W	5 kt E NE
06 02 79	A	32°00'00"S	104°30'00"W	10 kt NE N
06 03 79	A	30°00'00"S	106°00'00"W	15 kt N NE NW
06 04 79	A	30°00'00"S	110°00'00"W	20 kt N NW

^αA = anticyclonic.

* Wind information extracted from charts of low-level cloud stream lines.

TABLE III. Wind speed in knots and wind direction relative to the geographic north.*

Date MM DD YY	Type of Cell	Center of the Cell		Nearshore Wind Speed Direction
		Latitude	Longitude	
09 09 79	A ^a	29°30'00"S	80°30'00"W	5 kt E W
09 10 79	A	30°00'00"S	120°00'00"W	5 kt SE E
09 11 79	A	30°00'00"S	103°00'00"W	10 kt NE N
09 12 79	A	29°00'00"S	115°30'00"W	15 kt N NW
09 13 79	A	31°30'00"S	101°00'00"W	15 kt N NE
09 14 79	A	31°30'00"S	97°30'00"W	20 kt N NW
09 15 79	A	30°00'00"S	106°00'00"W	25 kt N NW
09 16 79	A	29°00'00"S	97°30'00"W	25 kt N NW

^aA = anticyclonic.

* Wind information extracted from charts of low-level cloud stream lines.

TABLE IV. Wind speed in knots and wind direction relative to the geographic north.*

Date MM DD YY	Type of Cell	Center of the Cell		Nearshore Wind Speed Direction
		Latitude	Longitude	
01 07 80	A ^a	30°00'00"S	110°00'00"W	20 kt N NW
01 08 80	A	30°00'00"S	100°00'00"W	20 kt N NW
01 09 80	A	32°00'00"S	90°00'00"W	15 kt N NW
01 10 80	A	32°00'00"S	87°00'00"W	20 kt N NW
01 11 80	A	25°00'00"S	130°00'00"W	15 kt NE N NW
01 12 80	A	27°00'00"S	130°00'00"W	15 kt NE N
01 13 80	A	27°00'00"S	130°00'00"W	10 kt N NE
01 14 80	A	30°00'00"S	120°00'00"W	5 kt N NE

^aA = anticyclonic.

* Wind information extracted from charts of low-level cloud stream lines.

TABLE V. Wind speed in knots and wind direction relative to the geographic north.*

Date MM DD YY	Type of Cell	Center of the Cell		Nearshore Wind Speed Direction
		Latitude	Longitude	
04 01 80	A ^a	29°00'00"S	100°00'00"W	10 kt N NW
04 02 80	A	31°00'00"S	108°00'00"W	10 kt E NE
04 03 80	A	35°00'00"S	100°00'00"W	15 kt NE
04 03 80	C ^b	40°00'00"S	75°00'00"W	5 kt E SE
04 04 80	A	34°30'00"S	98°00'00"W	15 kt N NE
04 04 80	C	45°00'00"S	127°00'00"W	15 kt NE E
04 05 80	A	28°00'00"S	98°00'00"W	15 kt N NW
04 06 80	A	26°00'00"S	90°00'00"W	10 kt E NE
04 07 80	A	25°00'00"S	102°00'00"W	10 kt N NE

^aA = anticyclonic.

^bC = cyclonic.

* Wind information extracted from charts of low-level cloud stream lines.

TABLE VI. Wind station locations along the coast of Chile.

N°	Name	Latitude	Longitude	Geography
1	Pta. Tortuga	29°56'00"S	71°21'00"W	Shore Point
2	Pta. Angeles	33°01'00"S	71°39'00"W	Shore Point
3	Constitucion	35°06'00"S	72°13'00"W	Shoreline
4	Pta. Carranza	35°34'00"S	72°38'00"W	Shore Point
5	Pta. Tumbes	36°37'00"S	73°07'00"W	Peninsula
6	Is. Mocha	38°25'00"S	73°54'00"W	Offshore Island

IV. DESCRIPTIVE ANALYSIS

Winter Season

The mosaic representing the winter season was taken on September 16, 1979. It is composed of six separate images which together represent a six-minute view of the area. The area covered by this mosaic extends from 28°S (Coquimbo Bay) to 39.5°S latitude (near Corral Bay) along the coast of Chile, extending offshore an average of 300 km (Figure 4).

Upwelling

Upwelling zones along the coast appear very well developed between Quele Bay (39.2°S) and San Antonio Bay (33.5°S). However, strongest upwelling areas are found from Quele Bay to Mocha Island (38.2°S) and from Constitución (35.5°S) to San Antonio Bay; the latter appears to be the most active upwelling area, extending offshore to about 40 km, apparently as a response of direct transport by Ekman drift. Nevertheless, the area between Mocha Island and the coast does not suggest a direct transport offshore by Ekman drift only, but by lateral mixing of coastal eddies as well. Within this area, and especially around Mocha Island, upwelled waters extend further offshore to about 60 km, taking the form of a developing cyclonic circulation or gyre, centered approximately 30 km offshore. The cyclonic circulation appears to increase gradually in size, to the west, where it mixes with the upwelled waters that originated around Mocha Island. As a result of this complex cyclonic



FIGURE 4. Mosaic of chlorophyll images along the coast of Chile. Orbit N°4526. September 16, 1979. Band-3 (550 nm).

circulation, coastal, near-coastal and oceanic waters appear to take part in the process. However, the differentiation between coastal, near-coastal and oceanic waters within this specific area is difficult to establish (it will be discussed later).

Between Santa María Island (37°S) and Constitución, the upwelled waters appear to be reduced to a narrow zone very close to shore. This is more evident in San Vicente and Talcahuano Bays (36.5°S-37°S), where the waters show a very low pigment concentration.

Between Valparaiso (33°S) and Coquimbo (28°S), the upwelling process is not evident. A strip a few kilometers offshore along the coast and covering very coastal waters (2 or 3 km) with a relatively high pigment concentration zone can be detected. It can be said that the upwelling process is almost absent in this area. Relatively low pigment concentration waters extend very close to shore within this area and they almost completely cover Coquimbo Bay.

Low Pigment Concentration Zone

The lighter area along the coast, which is interpreted as upwelled waters, is suddenly terminated offshore by a darker strip representing low pigment concentration waters (low radiance in band-3). This is denoted as the Low Pigment Concentration Zone (LPCZ) (Espinoza et al., 1983). LPCZ strip involves near-coastal waters and it extends further offshore in some places, intruding into oceanic waters. Oceanic waters are represented by the mid-range of radiance in band-3. They show lower pigment concentration

than upwelled waters but, at the same time, they show higher pigment concentration than LPCZ waters. Nevertheless, LPCZ waters show a remarkable difference in the pigment concentration compared with upwelled waters. This will be discussed later.

The area covered by the LPCZ strip is generally variable in width, with very narrow areas in places where distinct surface oceanic water intrusions appear to approach the shore. Wider areas occur where LPCZ water plumes extend further offshore. These places are: off Coquimbo (30°S), off Valparaiso (33°S), and off Talcahuano (37°S). The narrower areas extend just 10 to 20 km offshore from 31°S to 34°S latitude. In general, the LPCZ strip is present, parallel to the coast, along most of the area of study.

The southern boundary of the LPCZ strip appears to be represented by the complex circulation pattern present around Mocha Island, where a small-scale eddy dominates the surface circulation process. However, there is evidence of the presence of the same type of phenomenon (a LPCZ strip) as far south as Chiloé Island (43°S), which can be seen in a different chlorophyll image taken in a different time period, April 3, 1979 (Figure 5).

Three LPCZ plumes extending offshore are very distinctive structures, being better developed than that seen off Coquimbo. This offshore plume suggests an offshore coastal-water transport, and, as coastal upwelling appears to be absent in coastal regions within this area, the LPCZ plume extends from very close to shore to about 300 km offshore. That does not mean that LPCZ waters were or

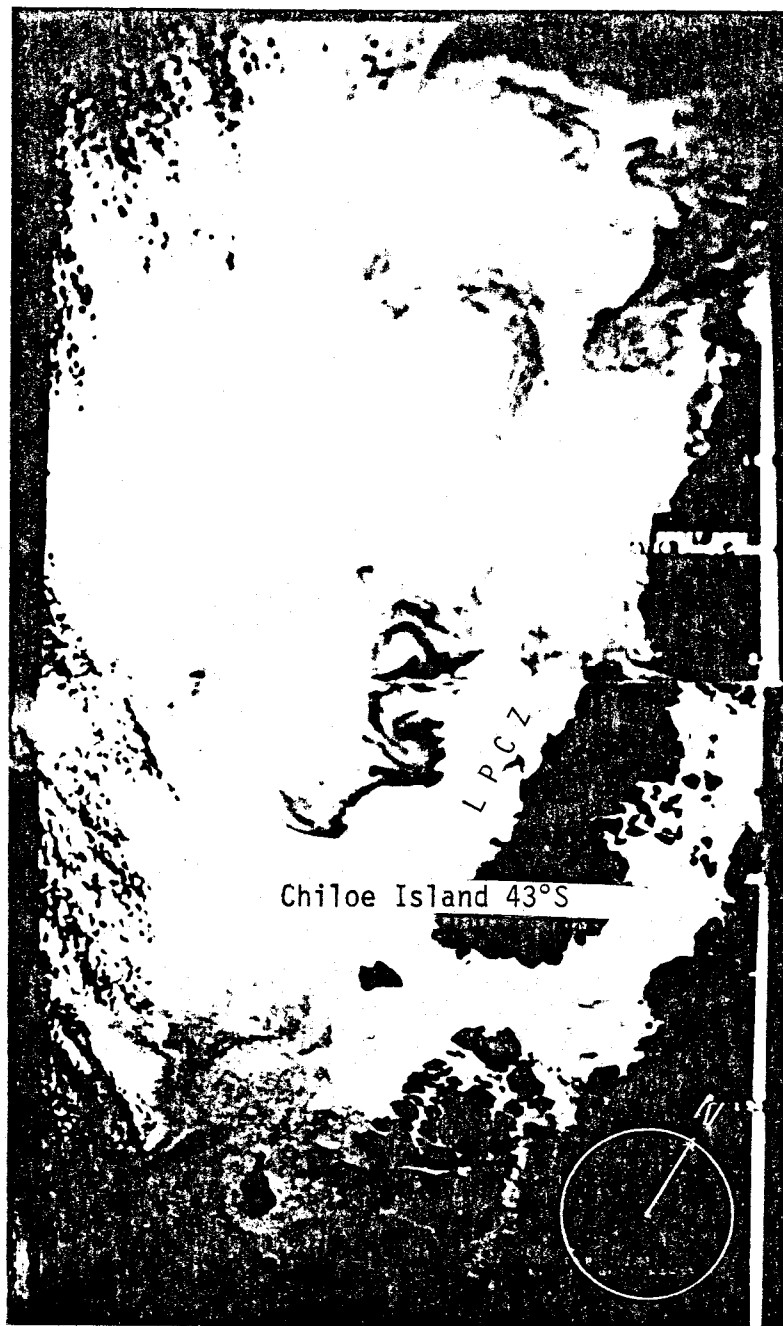


FIGURE 5. Small mosaic of chlorophyll images along the coast of southern Chile. It shows southernmost extension of LPCZ phenomenon off Chiloe Island (43°S). Orbit N $^{\circ}$ 2232. April 3, 1979. Band-1/Band-3 (443 nm/550 nm). Lighter areas are low pigmentation; darker areas are high pigmentation.

were not upwelled waters some time before. However, it is clear when the picture was taken, the LPCZ waters showed low pigment concentration, which we assume represents low chlorophyll content, as shown in some frequency ranges (Smith and Baker, 1982).

The head of this LPCZ plume appears to be decreasing in size as far as it extends offshore. This point is where oceanic waters appear to dominate the circulation pattern. Oceanic waters are distinguished by their relative high pigmentation, much lower than upwelled waters (lightest areas) but higher than the LPCZ waters, the darkest areas of the mosaic.

The LPCZ plume located off Coquimbo starts to develop a large-scale clockwise gyre involving oceanic waters at the edge of its head. This large-scale eddy does not appear to be as well-defined as a second large-scale eddy seen at the head of the LPCZ plume located off Valparaiso. The latter can be detected more clearly than the first one, but at the same time it presents a more complex configuration. This apparently occurs, in this case, due to the counter-clockwise eddy formation as a consequence of the strong interaction between the LPCZ plume coming offshore and the strong oceanic water jet intruding onshore, which does not occur off Coquimbo. As a consequence, the large-scale eddies formed at the head of the LPCZ plume off Valparaiso appear much better developed than the ones formed at the head of the LPCZ plume off Coquimbo. Nevertheless, the LPCZ plume off Valparaiso is less defined than the one off Coquimbo, but it can be clearly seen that it extends offshore as far as the

one off Coquimbo, about 300 km offshore.

A third LPCZ smaller plume appears extending off Constitución (35.5°S), but it is not so well developed as those located off Coquimbo and Valparaiso. This small-scale LPCZ plume seems to extend just 100 km offshore and does not appear to be involved in the clockwise, developing eddy seen at the head of an onshore oceanic water intrusion present within that specific zone. Another difference is that in this case the LPCZ plume is located between coastal upwelled waters coming offshore and oceanic waters apparently moving onshore. This situation is not evident in the other two plumes.

Coastal Intrusions of Oceanic Waters

As described earlier, the LPCZ strip for the September mosaic is broken by two major onshore intrusions of oceanic waters, clearly distinguished in two places: between Constitución and Valparaiso and between 30°S and 32°S, just south of Coquimbo Bay. The two intrusions have almost the same pigment concentration, which is higher than the LPCZ waters, but much lower than the coastal upwelled waters.

The northernmost intrusion is the lesser developed, but it appears extending closer to the shore until about 30 km off the coast. This coincides with the zone where the LPCZ strip has its narrowest state and also where upwelled waters (very light areas) occurs in a very narrow coastal strip. The head of the intrusion seems very flat and it appears to be oriented parallel to

the coastline. Nevertheless, a diffuse developing eddy structure can be detected at the edge of the jet head, this process appears to involve LPCZ waters. This could be a result of the interaction of offshore-onshore water transport. The onshore intrusion jet appears located in between the two major LPCZ plumes coming offshore. The eddy structures appear evident at different scales, as will be discussed later.

The southernmost onshore jet intrusion appears to be better defined. It intrudes to within some 80 km off the coastline showing the formation of two large-scale eddies at the northern and southern boundaries of its head. The two eddies appear to involve LPCZ waters and they appear to be coming from the major offshore LPCZ plume in the north and from the LPCZ strip in the south. That area is where the third (the smallest) LPCZ plume appears to be forming.

The southernmost eddy is cyclonic, and the northernmost is anticyclonic. This configuration results in the formation of a hammer head structure in the leading edge of the onshore intrusion jet (Espinoza et al., 1983).

The southernmost eddy is located further onshore and it involves LPCZ waters directly from the LPCZ strip. In that way, the LPCZ strip seems very diffuse in that specific area, apparently due to its involvement within the eddy structure. This also coincides with the area where upwelled waters extend farther offshore, suggesting that within that zone the coastal upwelling process is strong.

The orientation of the southernmost jet intrusion appears to be

more angular in respect to the coastline (about 45°) than the northernmost jet. The latter seems more perpendicular to the coastline. However, the general orientations of the two jet intrusions appear to be northeastward. The general orientation of the Chilean coast is south-north and as the images were taken in reference to the satellite orbit orientation, the geographic position of events is relative within the mosaic.

Autumn Season

Seven separate images, each of them showing different areas off the coast of Chile, compose the mosaic taken during the autumn season, April 7, 1980. It covers from 18°S (Arica) at the north (top of the mosaic) to 33°S (Valparaiso) at the south (bottom of the mosaic) and it covers an average of 350 km offshore (Figure 5).

Upwelling

As earlier stated, upwelled waters are represented by the lighter areas shown by the images. In this case, however, the structure is less clear than it was on the spring mosaic. Nevertheless, two well-developed areas of upwelled waters (lighter areas of the mosaic) can still be distinguished along the coast. The northernmost is located between Arica (18.5°S , the top of the mosaic) and Antofagasta (23.5°S). The southernmost is located between 27.5°S and 29.5°S , just north of Coquimbo.

Between Arica and Antofagasta, the mosaic shows the lightest

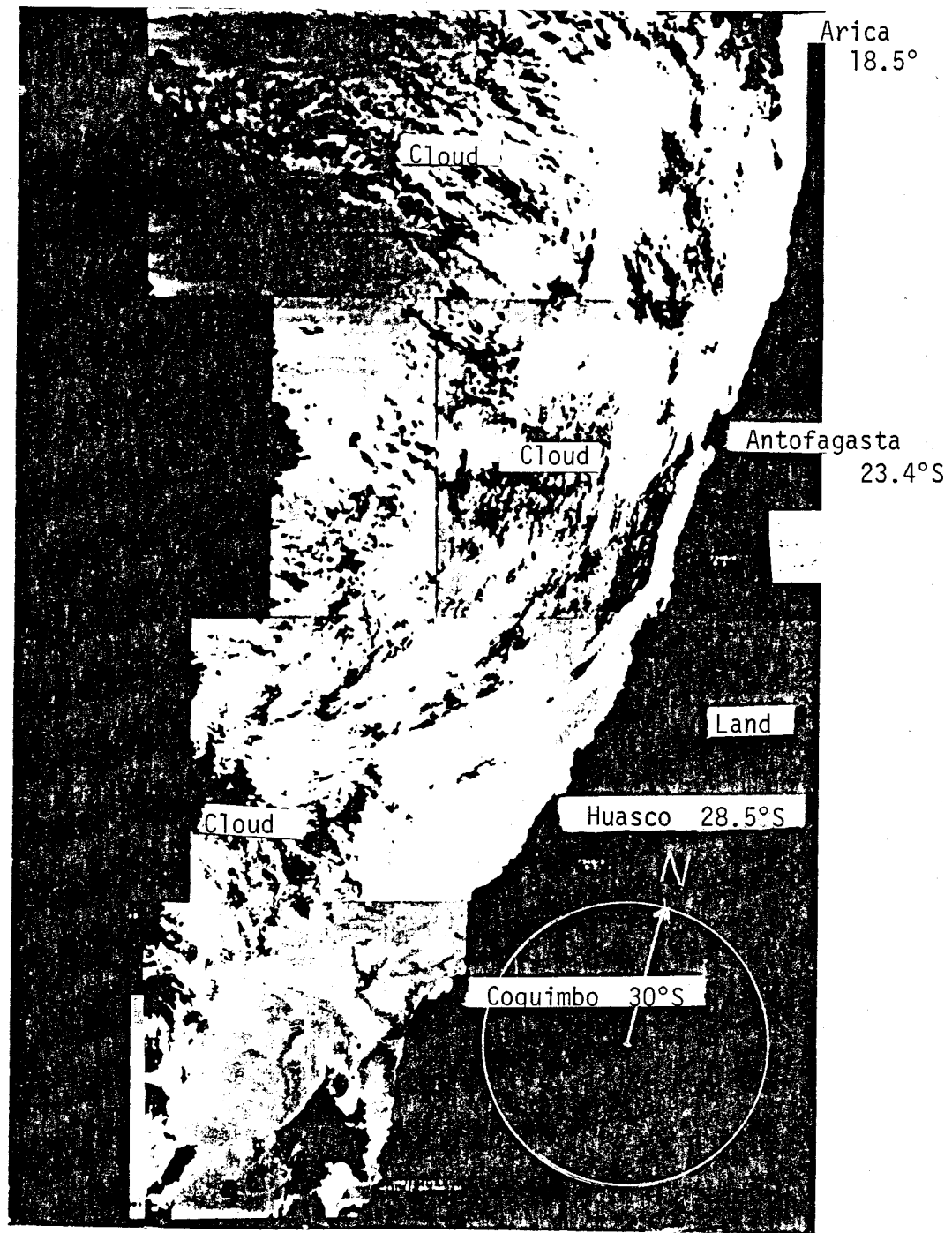


FIGURE 6. Mosaic of chlorophyll images along the coast of Chile. Orbit N°7345. April 7, 1980. Band-3 (550 nm).

(highest pigment concentration) area. Upwelled waters appear extending as far as 40 km offshore. From there to maybe 100 km, pigment concentration diminishes gradually until it shows the lowest value; this is interpreted as oceanic waters characteristics. These waters (darker areas) appear to dominate the area further offshore to the westernmost limit of the mosaic.

The southern boundary of this upwelling zone appears to be the Mejillones Peninsula. In that place, upwelled waters extend offshore in the form of a narrow strip to about 100 km. Within this specific area, the difference between upwelled waters (very light zones) and oceanic waters (darker zones) seems very clear.

The second area suggesting an active upwelling process, the southernmost, shows a different pattern than the one described above. It covers a wider area, from very close to shore to maybe 80 km offshore, but with a diffuse pattern of motion. Apparently, it cannot be a response to direct transport by Ekman drift but to some other mechanism, for example, a convergence zone formed by mesoscale gyres. As far as the images show, surface drift is poorly defined. Nevertheless, upwelled waters with high pigment concentration and near-coastal waters with relatively low pigment concentration can be distinguished clearly in both the southern and northern boundaries of this upwelling zone. In that case a convergence zone would be formed along 28°S, where the lighter areas of the mosaic can be seen. In this way, upwelled waters are the result.

The area between Coquimbo Bay and just north of Valparaiso

is relatively dark (low pigment concentration), suggesting very low or maybe no upwelling activity within coastal waters in that specific area. There is no evidence of a clear differentiation between coastal and oceanic waters. The seasurface pattern appears to be dominated by a relatively weak transport onshore of oceanic waters, which seem to extend to very nearshore zones, including coastal waters involved in eddy developing processes. These local eddies appear to be centered where surface waters show the lowest pigment concentration. The darkest areas are located off Coquimbo and along 31°S latitude.

The southernmost eddy appears to be taking the form of a small cyclonic gyre, with a diameter of approximately 80 km. The southernmost eddy suggests a counterclockwise developing formation, but it seems much less developed than the northernmost. Its size appears to be close to half that of the northernmost, i.e., about 40 km diameter. This type of structure is an unexpected feature.

The coastal zone between Chañaral and the Mejillones Peninsula (26.5°S - 23.5°S) shows relatively low pigment concentration waters, except for the presence of a small light spot, suggesting a relatively higher pigment concentration, located at 25°S . This lighter spot appears to be an extension of a local small-scale eddy located farther south, at the northern boundary of the upwelling zone located along 27°S latitude. However, the radiance (band-3) shown by that spot appears to be lower than the one shown by the lighter upwelled waters, described before.

Coastal Intrusions of Oceanic Waters

There are two areas where the shade scale of this mosaic suggests the presence of oceanic waters intruding onshore into coastal zones, at 27°S (the southernmost) and off Antofagasta (the northernmost). Both intrusions appear as developing small-scale eddies involving coastal upwelled waters. In both cases, the jet intrusions appear to be the boundaries of the two most active upwelling areas described above. The southernmost (27°S) seems to be intruding almost until to the shoreline itself.

In general, from 26°S to 18.5°S, the northernmost part of the mosaic, and westward from 100 km offshore, the surface pattern appears to be dominated by the presence of oceanic waters. Eddy structures and onshore-offshore water transport are not evident features in that area. The interpretation of the shade structure is very difficult due to the presence of clouds.

The southernmost area covered by this mosaic shows a different pattern of seasurface circulation compared with the rest of the mosaic. High pigment concentration waters appear to be extending from coastal regions to oceanic regions. In general, the patterns appear very diffuse. A weak onshore movement showing a wide developing front appears to be present from the west limit of the mosaic to about 100 km offshore and from the bottom of the mosaic to Coquimbo Bay (30°S). At its northernmost boundary, the front appears to be diminished by the eddy structure described before.

The southernmost boundary is covered by a large cloud (very black zone), which does not allow one to see the seasurface structure within the area.

Summer Season

The mosaic taken during the summer season, January 14, 1980, covers from 20°S (Equique) to 34°S (just south of Valparaiso) extending offshore an average of about 300 km (Figure 7). About 35% of the area shown by the mosaic is covered by dense clouds, mainly over oceanic regions at the center of the mosaic. All the northern area (from Chañaral to Iquique) is affected by a broad, somewhat diffuse cloud structure present within that area.

Upwelling

Two major lighter areas, representing upwelled waters, can be distinguished. The better developed are located between Valparaiso and Coquimbo. Upwelled waters (high pigment concentration) extend as far as 100 km offshore from Valparaiso northward to 31.5°S (south of Coquimbo Bay). Between 31.5°S and 30°S, an upwelled water plume extends further offshore, about 270 km. This plume shows a developing eddy structure in both the northern and southern limits of its leading edge. Onshore flows will be described later.

The northern side of the plume head has a clockwise large-scale

eddy, which involves oceanic waters. The eddy increases in size to the north, showing a diameter of about 70 km. The western boundary of the eddy appears more diffuse than the rest of its body but it still is clearly detectable.

The southernmost eddy is counterclockwise and it involves oceanic waters in its structure. In this case, the eddy appears to increase southward and it is larger than the northernmost eddy; it is about 100 km in diameter. The center of the eddy shows lower pigment concentration than its surrounding waters. The latter appear to be coming from coastal upwelling zones; the oceanic waters located at its center appear to be part of an onshore intrusion.

The general structure of the high pigment concentration water plume, and specifically its leading head, is the same structure shown by the southernmost onshore jet seen on the spring mosaic (September 16, 1979, Figure 4), mentioned earlier as the hammer head structure (HH). In this case, an offshore upwelled water plume intrudes oceanic waters of lower pigment concentration, developing two large-scale eddies at the leading edge of its head. On the spring mosaic, an onshore jet is intruding coastal waters, also forming two large-scale eddies. The southernmost of the two onshore jets seen in this mosaic also appears to have a hammer head structure at the leading edge of its head. Another similarity with the spring mosaic is an offshore plume of coastal waters between two major onshore jets of oceanic waters.

The southern and northern limits of the area covered by high

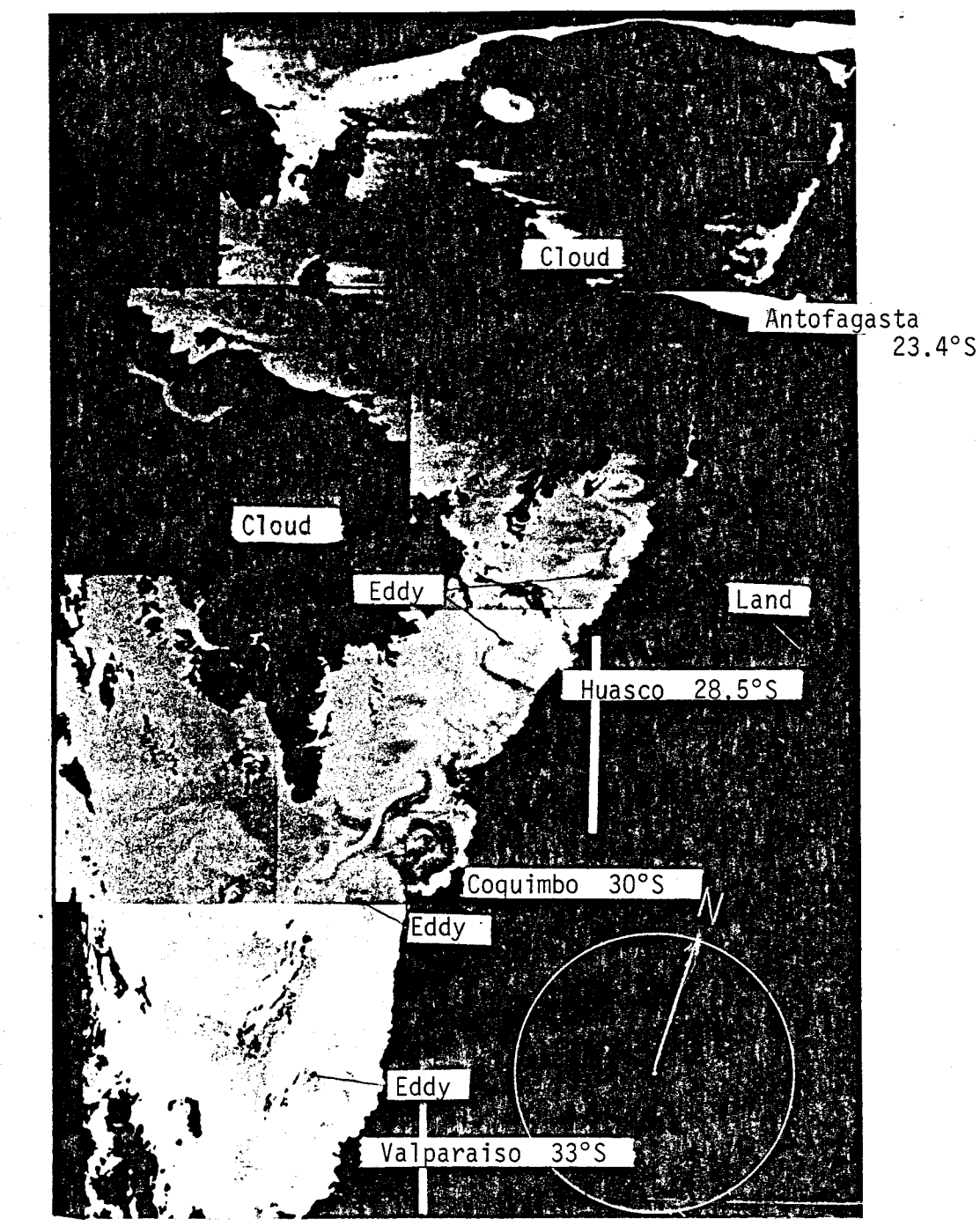


FIGURE 7. Mosaic of chlorophyll images along the coast of Chile. Orbit N°6184. January 14, 1980. Band-3 (550 nm).

pigment concentration waters, upwelled waters, appear to be dominated by two large-scale eddies. Both eddies involve waters with high pigment and low pigment concentration. These two eddies are located off Valparaiso and off Coquimbo, respectively. They will be described later as low pigment concentration zones (LPCZ).

The second area (the northernmost) showing upwelled waters (very light areas) is located between the northern link of Coquimbo Bay (29°S) and 27°S latitude (just south of Chañaral. This area is less extensive than the one described before and it shows a different circulation pattern. Lateral mixing by eddy structures appears to dominate the seasurface circulation process. Coastal and near-coastal waters appear to be involved in that process, showing different pigmentation in different parts of the eddy structures. One of the important limitations on the analysis of satellite products is present in this specific area; a large cloud is covering a major portion of the images (very black area). This leaves only an area about 150 km wide along the coast, available for interpretation.

A large-scale clockwise eddy is located off Huasco (27.5°S - 28.5°S). It extends from very close to shore to the easternmost limit of the cloud structure, about 150 km in diameter. Its center, located about 70 km offshore, shows a narrow strip of low pigment concentration waters following the clockwise sense of the eddy. The eddy itself appears to increase in size southward. Its northern limit shows a diffuse motion involving high pigment concentration waters. The cloud structure covering that zone makes its interpretation even less clear.

The southernmost limit of this eddy extends further southward and it coincides with the presence of another large-scale eddy involving low pigment concentration waters. The westernmost extension is limited by the large cloud structure mentioned before, although a relatively low pigmentation spot suggests the formation of another eddy but this time with a counterclockwise structure. The spot is located along 29°S and about 110 km offshore. Upwelled waters appear to be extending very far offshore but again the cloud structure does not allow one to see clearly its developing pattern. The eastern limit of this upwelled water area is represented by a low pigment concentration zone located along the coast from Coquimbo to 28°S. It cannot be said that this LPCZ water was not upwelled some time before; the explanation for the low pigmentation state shown in the images is not evident.

Low Pigment Concentration Zones

As stated earlier, low pigment concentration zones involving coastal and near-coastal waters (as defined on the spring mosaic description) are also present in this mosaic. In this case, they are found closer to shore than they were in the spring mosaic and also cover a smaller area.

Off Coquimbo, including the entire bay, a counterclockwise eddy involving low pigment concentration waters can be distinguished. Its center appears to be located about 50 km offshore from the center of the Coquimbo shoreline and bay. It has a diameter of about 90 km.

The LPCZ eddy extends northward in the form of narrow strip until it becomes involved in a developing clockwise eddy of upwelled waters described before. At this point, the LPCZ strip follows the clockwise sense of the developing eddy within the center of the body structure. That is where the LPCZ strip appears to be terminated. Again, large-scale eddies make up the major feature, dominating coastal and near-coastal waters in spite of the different pigmentation of the waters involved.

A second LPCZ structure is located just south of Valparaiso and it appears to be taking a form of a developing counterclockwise eddy, although its structure is not clear. However, a low pigment concentration strip extending northward can be clearly distinguished off Valparaiso. Just north of Valparaiso it becomes involved in another counterclockwise eddy which mainly involves upwelled waters within the outside of its body, but includes low pigment concentration waters at its center. A major onshore jet of oceanic waters, with a hammer head structure at the leading edge of its head, appears to be taking part in the circulation pattern as well. It will be described in the next section.

A major LPCZ event is found between Chañara1 (26.5°S) and the Mejillones Peninsula. At this point a large cloud structure makes any description impossible. Apparently, the LPCZ structure extends farther offshore, to about 200 km, and it is very poor in pigmentation. LPCZ waters appear to be extending very far offshore, maybe to the westernmost limit of the mosaic covering oceanic zones.

Nevertheless, as stated earlier, lighter and/or darker areas shown by the mosaic within this cloudy zone seem to be more a response to the cloud structure than a representation of pigmentation of sea-surface waters. If so, analysis of the northern half of the mosaic would not be valid for seasurface circulation.

Onshore-Offshore Surface Motion

Two major onshore intrusions of oceanic waters can be distinguished clearly within the oceanic area at the southern limit of the mosaic. The northernmost, and less clear, is located off Coquimbo. It extends from the western limit of the mosaic to about 130 km offshore, although cloud structure does not allow one to see clearly its greatest offshore extension.

The leading edge of the intrusion head appears to extend southward in the form of a circular motion. Nevertheless, its easternmost leading edge intrudes farther onshore in the form of a small LPCZ water strip, which apparently follows the external shape of the counterclockwise eddy of upwelled waters described before.

The southernmost leading edge of the intrusion head seems to be involved in the clockwise eddy formed by the leading head of the upwelled offshore plume extending off Coquimbo, which was described within the upwelling section. In general, this onshore intrusion does not seem very well-defined. More coastal developing eddies with opposite circulation interact strongly within this zone making the pattern a complex process to describe. Such patterns appear to be one of the relevant meso-scale events shown by these satellite

images. They are rarely found in earlier reports of surface circulation off the coast of Chile. As stated earlier, the differentiation in the surface water pigmentation is very clear as revealed in these chlorophyll images, but at the same time circulation patterns are likely dependent upon assumptions made on the correlation of radiance response and pigmentation of seasurface waters. This kind of dependency appears to be supported by the analysis of some chlorophyll images but this time showing the ratio of band-1/band-3 instead of band-3 (Figure 8).

The southernmost onshore intrusion, located off Valparaiso, seems to be better defined than the one just described. It extends closer to shore, maybe 100 km off the coast, where it is suddenly terminated by a strong zone of upwelled water. The meso-scale eddies can be distinguished at the southern and northern limits of the leading edge of the intrusion. The southernmost is clockwise while the northernmost is counterclockwise. These two eddies form a hammer head structure, similar to that seen on the leading head of the onshore plume of upwelled waters moving along 31°S latitude. Such a structure was also present in the southernmost onshore jet described from the September mosaic (Figure 4).

The northernmost eddy appears to be part of the major counterclockwise developing gyre formed by the upwelled offshore plume mentioned in the last paragraph. Again, low and high pigment concentration waters are involved within the same kind of seasurface circulation process. In this case a meso-scale eddy.



FIGURE 8. Mosaic of chlorophyll images along the coast of Chile. Orbit N°6184. January 14, 1980. Band-1/band-3 (443 nm/550 nm).

The southern limit of the hammer head structure seems less well-defined (Figure 9). The eddy is not as well-developed as the northernmost and apparently it could be involved in the counterclockwise eddy located at the southernmost extension of the upwelled area described before, just off Valparaiso. As was seen in the spring mosaic, major events dominating the seasurface circulation pattern are mainly large-scale eddy structures, which in most of the cases involve low and high pigment concentration waters.

End of the Autumn Season

Only three images form the mosaic taken during the last month of the autumn season. The purpose of including this small mosaic is not to represent each season with one mosaic but to show synoptic views of seasurface waters along the study area with enough time space to cover the slow time response of the ocean dynamics. This mosaic was taken on June 4, 1979, and it covers from 39°S to 31°S (Figure 10). As it has been on the other mosaics, part of the area covered by the images includes cloud structures. In this case the area free of clouds extends an average of about 180 km from the coastline and along the whole mosaic. Clouds are mainly present further offshore along the entire area covered by the mosaic.

Upwelling

This mosaic clearly shows a detailed pattern of the seasurface pigmentation. Upwelling activity can be detected within two specific areas along the coast, covering small zones very close to shore.



FIGURE 9. Hammer Head structure and associated eddy processes, revealed in the chlorophyll mosaic for January 14, 1980. Orbit N°6184. Ratio band-1 (443 nm)/band-3 (550 nm).

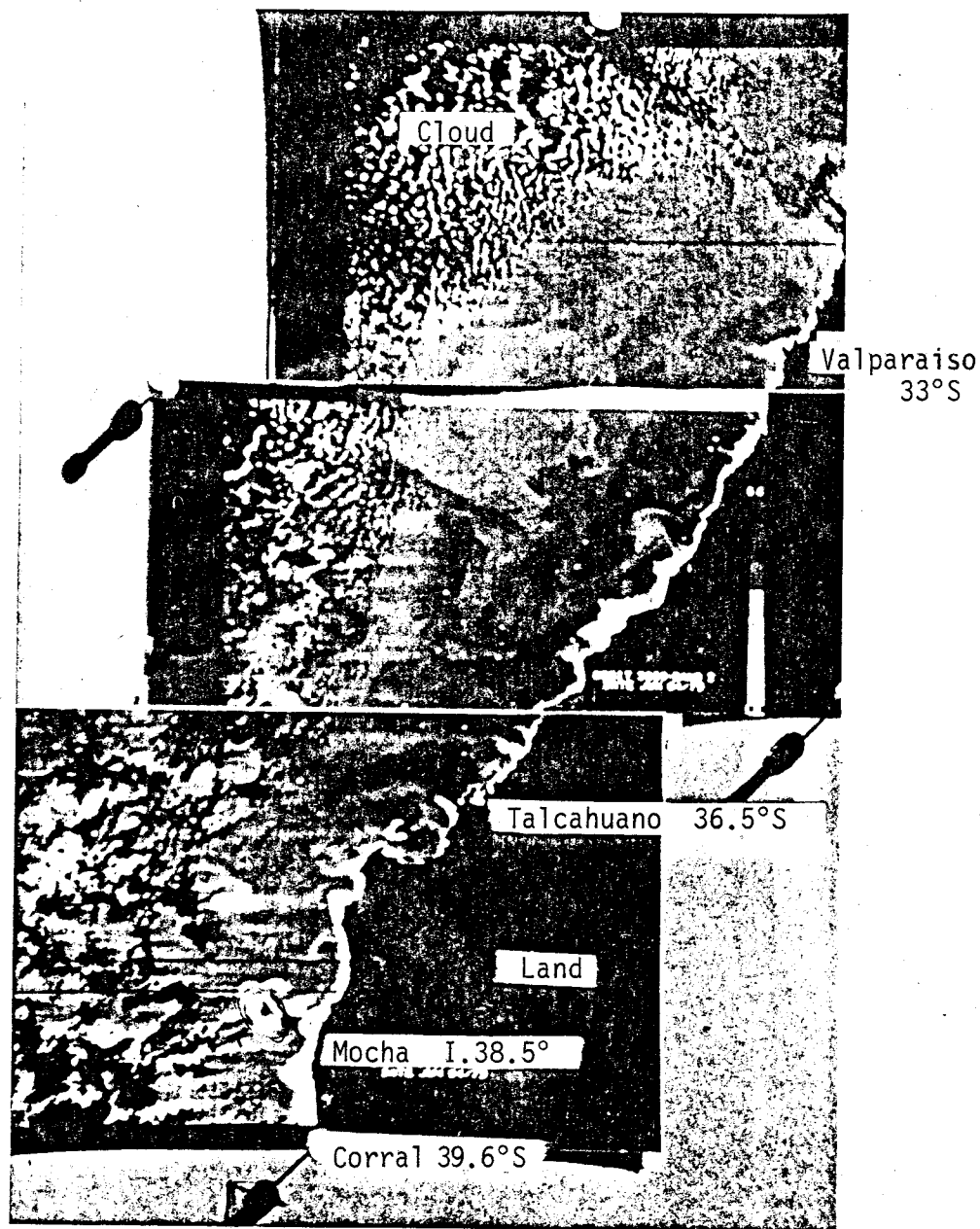


FIGURE 10. Mosaic of chlorophyll images along the coast of Chile. Orbit N°3089. June 4, 1979. Band-3 (550 nm).

The southernmost is located between the bottom of the mosaic (39°S) and Santa María Island (37°S). The northernmost extends from Constitución (35.5°S) to San Antonio (33.5°S) in the form of a very narrow strip alongshore.

The southernmost shows the most extensive lighter zone between Quele (39°S) and Mocha Island (38°S), about 20 km offshore. From there to Santa María Island lighter zones are reduced to a very narrow strip alongshore, suggesting low upwelling activity within that area. Between Mocha Island and the mainland, a small clockwise eddy seems to be present. This coincides with the pattern shown by the light zone around Mocha Island (high pigment concentration waters) which appears to be making a cyclonic movement around the island. This suggests that a larger eddy structure could be dominating the pattern between Mocha Island and the coast. The reason why this is not clearly seen in the image could be because the process is involving low and high pigment concentration waters, but with strong boundaries between them.

Santa María Island also shows a small light zone around it, but more poorly developed than around Mocha Island. The upwelled waters appear to be present just around the western side of the island, while the eastern side shows a very dark zone suggesting a very low pigment concentration, interpreted as the absence of upwelling.

The second area covered by high pigment concentration waters also appears very diminished in size. The more extensive zone is just north of Constitución, extending about 20 km offshore. From there to San Antonio, upwelled waters cover just a narrow strip

along the coast suggesting very low upwelling activity within that area as well. In general, the coastal pattern appears not to be very well-defined, as it was on the other mosaics.

Low Pigment Concentration Zones

Between Talcahuano (37°S) and Valparaiso (33°S), and immediately offshore of the upwelled zones, very dark areas can be distinguished. They cover an average of 100 km offshore being irregular in width. Off Constitución, the low pigment concentration zone appears to be broken by a narrow strip of relatively higher pigmentation in the form of a counterclockwise circulation; however, it does not appear to be very well developed.

In some places, like off Constitución and off Talcahuano, low pigment concentration waters seem to be moving southwestward but again the pattern is not very clear. It also could be the starting point of large-scale anticyclonic circulation gyres. The presence of the low pigment concentration zone itself is clear; it can be differentiated from oceanic waters because of their relative lower pigmentation and their location.

Onshore Intrusion of Oceanic Waters

Onshore intrusion of oceanic water is not as significantly evident within this mosaic as on the ones described before. There are two important points about this fact. First, the area shown by the mosaic does not extend so far offshore, especially from

Valparaiso to the south. Secondly, the westernmost limit of the mosaic is covered by cloud structure. These two facts limit the area of study to nearer the mainland than in the other mosaics. The southern half of this mosaic is limited to now more than 100 km offshore while the northernmost half shows about 50% more. However, off Valparaiso, the presence of relatively higher pigmentation waters, apparently terminated by the LPCZ strip, suggests a very weak on-shore intrusion of coeanic waters. Nevertheless, the picture is not clear because these mid-range pigmentation waters extend further northeastward to the shore. This coincides with the coastal area where apparently upwelled waters appear to be absent.

The mid-range pigmentation waters are also present from Talcahuano to the bottom of the mosaic, not including, of course, the lighter areas along the coast and around Mocha Island. The southernmost limit of the mosaic is dominated by the presence of clouds, which do not allow any interpretation of the seasurface pattern in oceanic waters.

Temperature Mosaic

Six satellite images in the thermal band compose the only temperature mosaic available for analysis. It corresponds to the same orbit as the mosaic of chlorophyll for September 16, 1979 (Figure 11). The area is exactly the same (28°S-39°S), covering an average of 300 km offshore. This alongshore mosaic shows seasurface temperature distribution for the study area. As it was on the chlorophyll

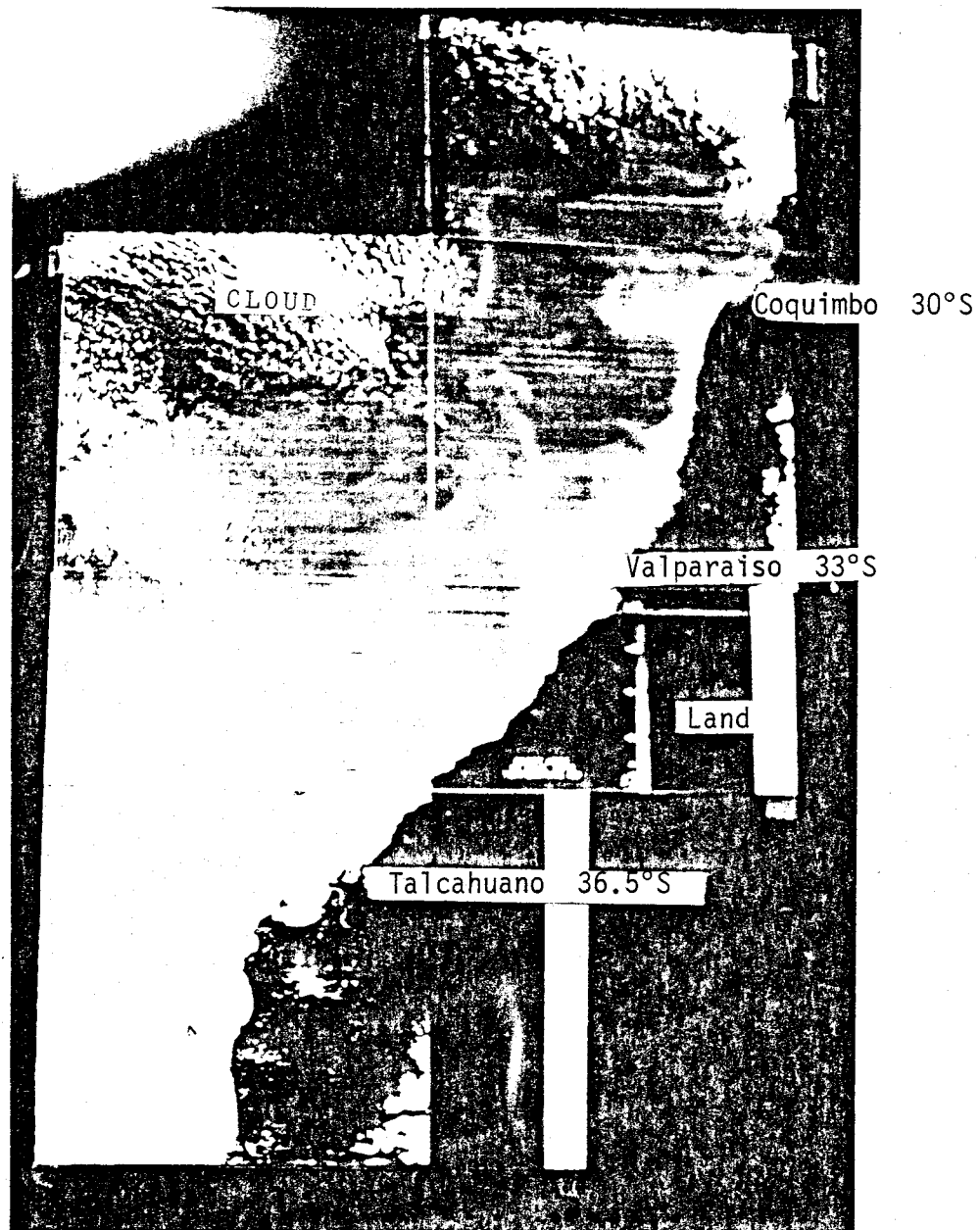


FIGURE 11. Mosaic of temperature images along the coast of Chile. Orbit N°4526. September 16, 1979. Band-6 (10.5-12.5 μm).

mosaic the westernmost limit of the mosaic is covered by clouds, as was the northernmost limit of it. In general, the temperature images are apparently less clear in showing seasurface circulation patterns. In spite of that, a clear differentiation between relatively colder and warmer waters can be distinguished.

Looking at the southern portion of the mosaic, a relatively cold surface water mass seems to be covering an extensive zone between Queule Bay and Constitución (39°S-35.5°S). It extends further offshore from the coast to the western limit of the mosaic, which in this case is represented by the cloud structure present within that area. The complex eddy structure revealed by the chlorophyll images around Mocha Island are not evident in the thermal images. Apparently that complex pattern occurs within a very narrow range of temperature (the brightest zone shown by the thermal mosaic).

The exception to that feature appears to be represented by a diffuse cyclonic large-scale gyre, apparently in a developing process, which can be detected about 120 km off Constitución. It includes mainly relatively cold water on its body, but a narrow warmer water strip can be distinguished within the easternmost extension of the eddy.

All of those coastal and near-coastal structures seen in the chlorophyll mosaic, like local eddies, upwelling zones and the LPCZ strip, apparently exist in a very narrow temperature range as well, hence are not resolved in the thermal images. Relatively cold waters cover the areas where those events were located within the

chlorophyll images. This relatively cold water area extends along the nearshore from Talcahuano to Coquimbo (37°S - 30°S). It varies in width approximately between 30 km and 60 km, extending across the sharp front between upwelled waters and the LPCZ.

Two relatively cold water offshore plumes can be distinguished, off Coquimbo--the northernmost, and off Valparaiso--the southernmost (30°S - 31°S and 33°S - 34°S , respectively). These two plumes correlate very well in position with those LPCZ offshore plumes described on the September chlorophyll mosaic. Again the coastal upwelled waters and LPCZ waters appear to form only one relatively uniform body of relative cold water. This pattern of low and high pigmentation waters in a region of very small temperature range, suggests that the explanation for the presence of the LPCZ between upwelled waters and oceanic waters could be found within the biological activity rather than within the physical dynamic.

Two major tongues of relatively warmer waters appear to be intruding further onshore within coastal zones. They correlate fairly well with the two major onshore intrusions of oceanic waters seen on the chlorophyll mosaic. The northernmost of these two onshore tongues (30.5°S - 31.5°S) is better defined in the thermal mosaic than the southernmost one. This is the opposite situation of what the chlorophyll images show. The northernmost tongue involves relatively warmer waters while the southernmost shows a more diffuse temperature structure. The latter appears to be in a temperature range closer to that shown by coastal waters, relatively colder waters,

rather than the range shown by warmer oceanic waters. However, it is still clear that it involves warmer waters than upwelling zones do. Furthermore, a darker strip (relatively warm water) can be distinguished about 30 km offshore between Constitución (35.5°S) and San Antonio (33.5°S), which coincides with the position of the easternmost extension of the southernmost cyclonic eddy developed at the leading edge of the southernmost onshore intrusion shown in the chlorophyll mosaic.

The rest of the intrusion body appears to be in a very narrow range of lower temperature, but still it seems warmer than upwelled waters located within coastal regions and at the southern part of the study area.

As stated earlier, the thermal images appear to be less clear in showing surface circulation patterns than the chlorophyll images, but at the same time they represent a very good complement to them.

V. DISCUSSION AND CONCLUSIONS

The detailed patterns of seasurface chlorophyll, a distribution shown by the four mosaics analyzed, provide a basis for a tentative description of three major features of the coastal and near-coastal seasurface circulation patterns off the coast of Chile. Upwelling areas, onshore-offshore surface drifts, and large- and small-scale eddy structures seem to be the dominant features within large extensions of the study area. A fourth unexpected feature observed in the images was low phytoplankton pigment concentration zones located between coastal upwelled waters and oceanic waters with relatively highly pigmentation. These transition zones in the seasurface pigmentation in the mosaic taken in September 16, 1979, extend almost along the entire area covered, suggesting not only a physical process but a biological process as well.

The September mosaic (Figure 4), the transition between winter and spring seasons, is the clearest of the four. It presents the largest areas free of clouds and, on the other hand, the best developed features of the seasurface water motions. Upwelling zones are clearly limited to coastal waters. In some locations the upwelled waters extend farther offshore, apparently not only as a result of direct offshore transport by Ekman drift but also by lateral mixing processes due to eddy structures which appear to dominate within these coastal regions.

The general pattern of low-level wind shown by the meteorologic charts for the preceding week (Appendix C), the September mosaic,

suggests favorable conditions for upwelling, especially between 31° and 38°S latitude. A large anticyclonic cell centered at about 30°S latitude and 125°W longitude is present within the six-day period. Coastal and near-coastal wind vectors indicate certain constancy in the direction and strength of the wind which flows northward between Talcahuano and Coquimbo. The wind speed is between five and fifteen knots within the first three days, increasing gradually to twenty-five and thirty knots within the last three days before the date of the mosaic.

A transition zone on the wind direction appears along 40°S latitude where the main direction seems to be eastward, apparently due to the presence of a cyclonic cell moving northward from higher latitudes. South of 40°S, southeasterly and southerly winds appear to dominate the area.

The winds within the last days preceding the mosaic coincide with the well-developed upwelling zones shown by the chlorophyll mosaic. However, the poorly detailed pattern of small-scale circulation does not allow any interpretation of the onshore-offshore water intrusions and their associated large-scale eddies (hammer head structures).

The temperature mosaic (Figure 11) also shows evidences of upwelling within the coastal region between Talcahuano and Coquimbo. Relatively colder waters extend not only along the coast but as large-scale offshore plumes as well. This temperature distribution suggests that upwelled waters and low pigment concentration waters were within a very narrow temperature range. The winds derived from

low-cloud vector map appear strong enough to support the idea of colder waters moving, uncommonly, so far offshore. Nevertheless, the low pigmentation waters are clearly indistinguishable within the temperature mosaic. It shows that within about 200 km off the coast, the temperature varies gradually from cooler to warmer with the exception of those locations where eddy development takes place. On the other hand, the chlorophyll images show a transition zone (LPCZ) between high- and mid-range pigmentation moving from upwelled waters in coastal regions to oceanic waters intruding onshore. This, together with the large extension of the LPCZ, makes it very difficult to associate these low pigmentation waters with a specific water mass.

The analysis of this phenomenon depends so far upon certain limitations within the use of chlorophyll images centered at one band of radiance response. Even though the correlation between ship-board data measurements and estimations derived from satellite images has been shown as high by several authors (Smith and Baker, 1982; Smith et al., 1982; Gordon et al., 1983), still it apparently depends upon the time differential between the satellite and ship measurements (Smith et al., 1982). Moreover, the relationships have been calculated for specific areas, which also limits the interpretation of the remote sensed data (off California and Mid-Atlantic Bight).

Considering all these limitations, a better understanding of the upwelling processes of the study area, including physical dynamics, population dynamics of plants, and grazing activity by herbivores, could provide a basis for explaining the LPCZ phenomenon. There are

some evidences, detected within upwelling zones on the Oregon coast, that indicate that the presence of such LPCZ can be the result of severe grazing by herbivores. This activity could reduce the phytoplankton density within specific areas by one or more orders of magnitude. Such a difference could be the one between LPCZ waters and upwelled waters shown here. The determination of time responses of phytoplankton growth to strong winds favorable for upwelling and the biological activity that takes place following the cessation of the wind could also be a key for the explanation. Short time response of upwelling processes when intensification of the wind field occurs has been observed by several authors (e.g., Breaker and Gilliland, 1981). Could the LPCZ waters be old upwelled waters? If so, how can they extend as far as hundreds of kilometers offshore like the plume extensions seen here? Why does the difference in pigmentation between LPCZ and upwelling areas appear so abrupt in space? These are major questions which, unfortunately, cannot be achieved from these limited data.

As stated earlier, the LPCZ phenomenon has been detected in the same kinds of images but taken on different orbits and dates. The mosaic taken in January 14, 1980 (Figure 6a) shows a well-developed LPCZ located at the Bay of Coquimbo (30°S). The structure present in this case is an anticyclonic eddy which covers the entire bay. The other major difference is that here the LPCZ definitely lies within coastal upwelling zones. Just north of Coquimbo, a second but less well-defined LPCZ is detected. It also appears to be

involved in an eddy but with a cyclonic form. This mosaic does not show the LPCZ strip structure seen in the September mosaic, in general the picture is different as well as the area covered. Nevertheless, the evidences for the same kind of phenomenon show up clearly.

The low-level wind charts also show a different situation compared to the September one (Appendix C). The large anticyclonic cell was then centered farther offshore and northward (25°S and 130°W). The wind was strong during the first three days preceding the mosaic, between 15 and 25 knots, along the near-coastal regions with the predominant direction northward-northeastward between Valparaiso and Arica (33°S - 18.5°S), suggesting a favorable situation for upwelling. Within the last three days preceding the mosaic, a cyclonic cell moved in from higher latitudes and a cessation of the wind event occurred. Wind speed diminished to less than five knots and the direction was northward from 29°S in the north and mainly southeastward from 30°S southward. Along 29.5°S a transition zone took place with winds blowing mainly eastward. Within coastal and near-coastal regions, this transition zone covered wider areas centered approximately along 30°S (Table IV).

The atmospheric situation, involving a cessation of wind and small-scale spatial changes in the speed and direction over coastal and near-coastal regions, suggests favorable conditions for the formation of those coastal eddy structures seen within the January mosaic. The particular situation where coastal eddies show anticyclonic form south of Coquimbo and cyclonic form north of Coquimbo

appears to agree with the low-level wind pattern. Apparently, those small-scale spatial changes in the wind field would be stronger at the surface, but the meteorological charts do not show these small-scale features of the wind field.

A similar situation can be associated with coastal eddies located around Mocha Island and Talcahuano September mosaic. The low-level wind charts for that period show a transition zone of the wind field covering coastal regions centered along 40°S (Table III). This also coincides with a well-developed upwelling zone revealed by the mosaic within the transition area of the wind field. However, the upwelling seems less developed than the one shown by the January mosaic. This difference appears to be related to the time response of the water motion to the wind stress. The September mosaic apparently is within the wind event period, while the January mosaic is just after the cessation of the wind. This suggests that during strong winds, surface waters may be measurably poorer in phytoplankton pigmentation than during the period just after the cessation of the wind event, at which time solar stratification of surface water sets in and strong phytoplankton blooms occur.

In the mosaic taken April 7, 1980 (Figure 6), LPCZ phenomena are not clearly detectable. However, a transition zone within the seasurface water motion appears clearer than in the other mosaics. The cloud motion seems very clear. It suggests that an anti-cyclonic motion dominates the area north of Coquimbo while a cyclonic one would dominate south of Coquimbo. The transition zone

would be located again along 30°S ; in this case this also coincides with a very well-developed upwelling area within coastal eddies dominate the sea surface circulation pattern within this transition zone.

The low-level wind charts for this period show a more complex pattern than for the others (Table V). The anticyclonic cell appears centered along 25°S and 110°W but it covers a reduced area. During the first three days preceding the mosaic, a cyclonic cell appears within coastal regions and centered along 50°S but it moved to the north during the following three days to 30°S , by this time over the mainland. On the other hand, the anticyclonic cell moved closer to land along 25°S . Again, a transition zone can be detected within coastal regions around 29°S . The wind speed was fairly constant (between 10 and 15 knots) while the direction appeared very unstable, varying between northeast and east from 25°S to the north and between east and east-south from 30°S southward.

The agreement between the mosaic and the meteorologic charts is in this case more evident than in the other cases, even though small-scale features remain as the major problem in the interpretation of the low-level wind-vector charts.

Low pigmentation zones are also detectable in the mosaic taken June 4, 1979. In this case, although the feature is less clear than within the other mosaics, the LPCZ phenomenon seems to have a pattern very similar to the one seen in the September

mosaic. The LPCZ is located between upwelled waters and oceanic waters with relatively higher pigment concentration. Nevertheless, upwelling is still detectable to some extent, the mosaic shows a poorly developed activity within the seasurface water motions, suggesting a very low wind activity during the period preceding the orbit pass. This coincides with the general pattern shown by the low-level wind charts for the period (Table II).

A large anticyclonic cell was centered at about 30°S and 105°W extending from 10°S to 50°S. Streamlines appear distant from each other during the four days resulting in low wind speeds within coastal regions, less than five knots. Within the last two days preceding the mosaic, the wind speed increased to about 15 knots coinciding with a better-defined pattern of the anticyclonic cell. On the other hand, the wind direction appears very unstable during the first four days (mainly northeastward) being better defined during the last two days (mainly north-northeastward). This suggests that the wind event started to develop within the last two days preceding the mosaic and with relatively low strength. This coincides with the poor activity of seasurface circulation pattern seen in the mosaic.

A second major feature of the seasurface water motion seen in the chlorophyll images are the onshore-offshore intrusions and their associated large-scale eddies within their leading heads (the hammer head structures). These features appear to be

well-developed in the September mosaic in two specific locations, as described before. A similar structure is also seen within the mosaic taken January 14, 1980, but it is not detectable in either the April mosaic or the June mosaic.

The temperature mosaic from the same orbit and covering the same area of the September chlorophyll mosaic indicates that these oceanic intrusions involve relatively warm waters. On the other hand, it shows that the offshore LPCZ water extensions are relatively cold waters which probably are old upwelled waters moving offshore due to direct transport by Ekman drift. Apparently this would also be the case within the January mosaic where upwelled (high pigment concentration) relatively cold waters extend farther offshore while mid-range pigmentation waters (probably warmer waters) intrude onshore, forming a dual versus single intrusion system, the same pattern seen in the September mosaic (Figure 4).

A similar temperature pattern (dual versus single intrusions) was shown by Inostroza (1972). He presented temperature maps showing average surface temperatures for each season based on data obtained in 36 cruises carried out between 1958 and 1968 (Figure 12). In the spring season, two large-scale warmer tongues intrude onshore between Coquimbo and Los Vilos (30° - 32° S) and between Valparaiso and Talcahuano (33° - 37° S). The latter is also present at the 50 m level (Figure 13), but it disappears at the 100 m level (Figure 14; both figures also from Inostroza, 1972).

The apparent correlation between these intrusions of oceanic

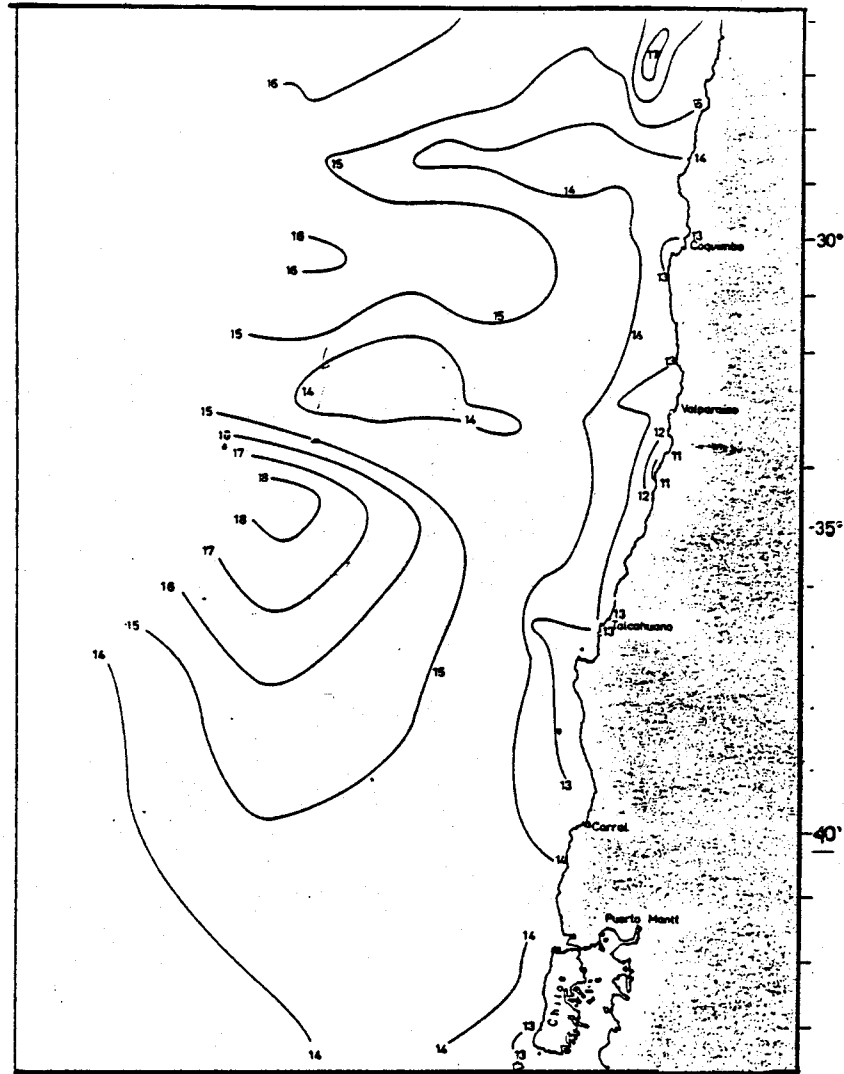


FIGURE 12. Average sea surface temperature off the coast of Chile. Spring season (from Inostroza, 1972).

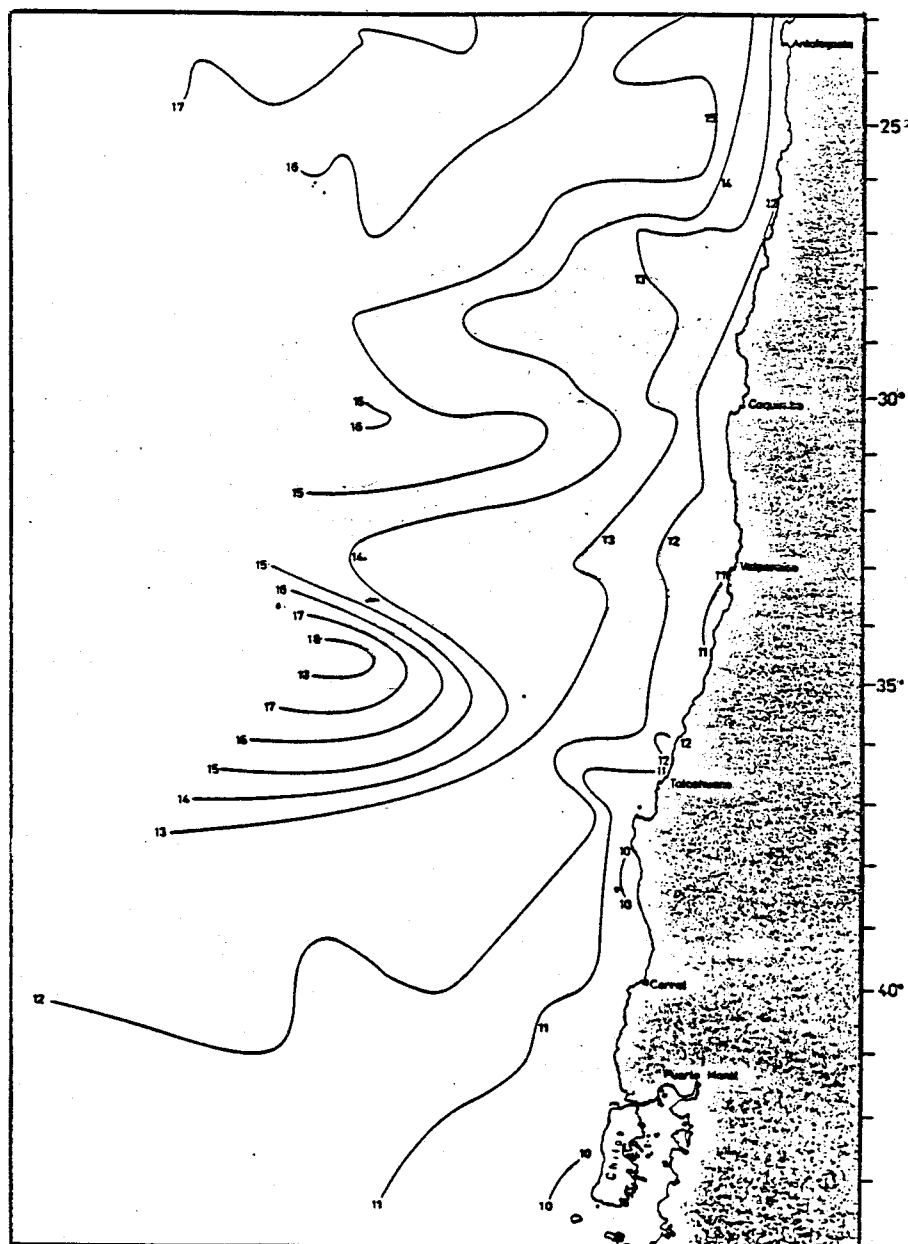


FIGURE 13. Average 50 m depth temperature off the coast of Chile during Spring (from Inostroza, 1972).



FIGURE 14. Average 100 m depth temperature off the coast of Chile during Spring (from Inostroza, 1972).

waters seen in the satellite images and the hydrographic data summarized by Inostroza (1972) suggests that the intrusions are semi-permanent features which would vary seasonally. This is supported to some extent by the January mosaic where the feature is also detectable. The hammer head structures seen at the leading edges of the intrusions are apparently a direct result of the interaction between the dual versus single offshore-onshore transports. Nevertheless, these features are not evident within the historic data presented by Inostroza (1972); they appear to be a semi-permanent feature of the seasurface circulation pattern of the study area, as it can be determined from the description of both the September and January mosaic. Are these offshore-onshore motions part of the Humboldt Current system? Or, do they represent a short-time scale response to spatial and non-uniform wind-driven force mechanisms? Could this feature represent a direct inflow from the West Wind Drift? The answer to these questions does not appear obvious.

Silva and Neshyba (1977) described a division point of the West Wind Drift as it approaches the Chilean coast along 40° to 44° S latitude. They also identified a stagnation point against the coast within these latitude limits. From the analysis of mean (summer conditions) dynamic topography they give evidence supporting an origin of at least part of the Humboldt current (the coastal branch) around 42° S and about 50-60 km off Chiloe Island. On the other hand, Neshyba and Mendez (1975) suggest that the West Wind Drift may bifurcate much farther offshore, perhaps as much as 100 km,

with the northernmost part of the bifurcation curving gently to the north while it approaches the Chilean coast at about 30°S. The southern part of the bifurcation is seen in the dynamic topography analysis made by Silva and Neshyba (1977) as the flow that executes the sharp curvature near Chiloe Island. The Neshyba and Mendez study was based upon satellite derived seasurface temperature maps. Their interpretation of the isotherm patterns suggests that a cyclonic eddy would occur between 33°S and 36°S latitude with an onshore flow within its northernmost limit (that eddy is also reported by Silva and Neshyba, 1977). This feature would be fairly consistent with the southernmost intrusion seen in the September mosaic. The large cyclonic eddy should have an offshore flow at its southernmost limit, which coincides with the evidence of a counter-flow within the West Wind Drift reported by Neshyba and Fonseca (1980).

Probably a better explanation for the occurrence of the onshore intrusions, shown by the chlorophyll mosaics, could be in the variability of wind stress patterns over this broad study area, especially for those detected off Coquimbo in both the September and the January mosaics. Periods of strong southwesterly winds alternating with weaker and reversed winds could generate favorable conditions for the occurrence of intrusions during the periods of relaxation. Nevertheless, as the historical data presented by Inostroza (1972) show a semi-stationary condition for the warm onshore tongue intrusions, a similar condition of stability for the wind stress pattern might be expected in the long-term average. The analysis of the true

wind field for the area covering the mosaic periods would be very helpful for future work.

The low-level wind charts covering the periods of those mosaics where the intrusions were detected do not strongly support the occurrence of the intrusions. Wind stress is not as strong as it would be expected to be and again the scale representation would be a problem to solve for a better interpretation of smaller-scale features. However, the stationary feature of the transition zone between the cyclonic and anticyclonic cells, which in both mosaic periods (September and January) dominated the general pattern, could support to some extent the presence of the onshore intrusions detected off Coquimbo. In any case, this explanation needs stronger evidence.

As stated earlier, coastal wind field measurements were not available for the time period analyzed in this study. Instead, it was considered useful to include nine months time series wind data, taken from coastal stations along the coast of Chile during 1977. The data for the spring season are missing (October to December). Wind vector diagrams are shown in Figure 15. At this point, it is useful to point out that 1977 is the year following the 1975-76 El Niño event, which apparently caused considerable changes in the meteorological pattern of the southeast Pacific, as well as in the oceanic pattern. Thus, it would be expected that this year (1977) could not be representative of the regular conditions of the area (personal conversation, William H. Quinn).

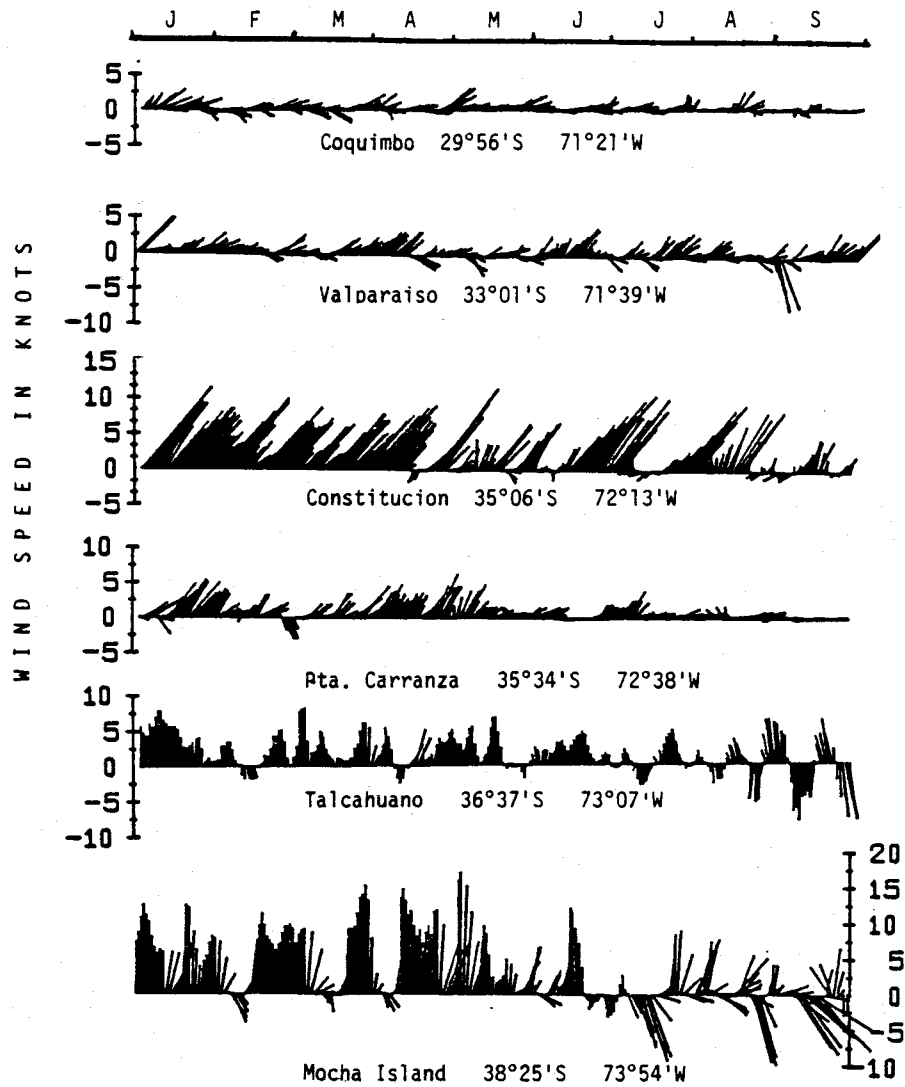


FIGURE 15. Wind time series for six stations along the coast of Chile. Nine months for 1977. Diurnal frequencies have been filtered.

In general, the station at Coquimbo shows very weak wind strength during the whole period from January to September, less than five knots. The wind direction appears unstable during the austral summer (January to March), varying from northeastward to southeastward. This situation changes during the rest of the period, autumn and winter seasons. At the same time that the wind became even weaker, it showed a main direction to the northeast. Characteristically starting in autumn, a certain periodicity can be detected within a monthly frequency of northward (less than 5 knots) wind peaks. Between those peaks the wind appears to be eastward during the autumn and early winter, with very low speeds as well, decreasing to almost zero at the end of the winter season.

This pattern of coastal winds does not support the features seen within the chlorophyll images. On the other hand, it shows a general weak wind strength as well as the low-level wind charts did. This is an unexpected situation for that zone where well-developed upwelling zones are detected within the mosaics, suggesting the occurrence of stronger winds. A similar situation can be seen at the Valparaiso station. In this case, the tendency seems to be more northward than in Coquimbo but with similar weak speeds. The exception occurs during the winter where the wind is stronger, large changes in direction. Again, the general patterns do not support what was described from the mosaics for that area.

At the Constitución station the conditions change very much. The stronger wind pattern, about ten knots, mainly northward, breaks with the variability shown in the other two stations. However,

southerly winds seen during the summer are more reasonably expected for that season. On the other hand, the conditions for the two following seasons are not. The normal stormy conditions for the winter season are absent here, which is also an unexpected result.

The station at Pta. Carranza shows a sort of transition between the rest of the stations. The wind is again very weak during the whole period with some constancy during summer and autumn, mainly northward, and in winter it changes to be mainly eastward and even weaker. This would provide some evidence for the transition zone between the high and low cells during the winter, but again the stormy conditions are absent in this season.

The last two stations show a similar pattern in the direction of the wind. The southernmost shows a much stronger wind field. The Mocha Island station is located about 25 miles offshore so it would seem to offer a better representation of surface winds than any of the rest of the stations. In these two cases the winter conditions are more representative of what can be expected for that season. Stormy conditions are fairly evident during the winter. A periodicity of strong southerly winds during the summer and autumn, with that abrupt reduction in the wind strength between them, suggests favorable conditions for upwelling and for the occurrence of coastal eddy structures due to the abrupt changes in the wind speed, represented by the cessation of the wind.

Within such conditions, the occurrence of onshore intrusions could occur as well. This unexpected pattern of the coastal wind

field agrees with the evidence for considerable changes in the oceanographic conditions reported by Uribe and Neshyba (1983) and also mentioned by Quinn (personal conversation). As stated earlier, better results can be achieved from the analysis of these kinds of wind data related to the satellite images. Much work remains to be done in the use of these kinds of satellite products; their utility appears extremely evident.

VI. APPLICATIONS OF CZCS NIMBUS-7 REMOTE SENSED DATA IN CHILE

There are important implications to coastal and near-coastal fisheries in this initial analysis of chlorophyll and temperature images off Chile. The existence of persistent but probably episodic intrusions of oceanic water and large-scale offshore extensions of upwelled water plumes, can influence the patterns of populations of migratory fish. The presence of the LPCZ may have an important influence upon the population patterns of the herbivore species, and thus indirectly control the behavior of larger predatory animals.

Before going any further, it is necessary to point out what would be the estimated steps to follow to complete the development of techniques and algorithms which are necessary to make these satellite products a useful tool in the fishery resource management.

First, a bio-optical technique which allows the classification and optical modeling of natural waters of the area must be done. This study could be achieved by the use of techniques already developed for natural waters in general but carried out in other areas, or it could be made specific to waters within the area of interest. The objective would be to optically classify the Chilean coastal waters and to construct a predictive model of these waters in terms of the total chlorophyll-like pigment concentration. A bio-optical classification model would provide an index of spectral irradiance data in terms of the primary biogenous factors

influencing the optical properties of the seawater analyzed. A knowledge of that would permit calculation of the spectral radiant energy penetrating the seasurface layer.

Secondly, an algorithm relating the spectral irradiance of the sea water measured by the satellite sensor with real chlorophyll concentration should be done. This would permit the use of chlorophyll images in the determination of total phytoplankton pigment concentration. With this, an attempt to determine primary production in terms of biomass could be carried out.

The Chilean fishery is a very important factor in the economy of the country. The occurrence of natural phenomena on one side and problems in management on the other has resulted so far in strong irregularity in the industrial fishery production. A better knowledge of the physical and biological processes which govern the Chilean waters is necessary to gain optimum production. Migration regimes of the most important species in terms of determination of high productivity areas and meso-scale surface and nearsurface circulation patterns may lead to improved methods for managing and exploiting fisheries.

An example of this kind of problem is the fishery of one of the three most important species within Chilean fisheries, JACK MACKEREL (Trachurus murphyi), common name Jurel. There are evidences of the presence of about 200 fishing boats--Russian and Polish--catching and processing that specie off Chile. They are concentrated in a specific area between 200 and 400 miles offshore

and between 36° and 41°S latitude (Figure 13). This zone is characterized by the presence of a temperature front of about 1°C/22 km, discussed by Neshyba and Fonseca (1980), as evidence of a counter-flow to the West Wind Drift off Chile.

Why is this specie, which is part of one or more coastal species, found so far offshore? Is this zone part of the migration areas and, if so, why? It also could be a part of the juvenile versus adult distribution pattern within that zone.

Evidence of offshore plumes of upwelled waters with high phytoplankton pigment concentration are clear in the chlorophyll images, specifically in the January mosaic. Moreover, from the Chiloe image, it is clear that physical processes also involve offshore plumes of coastal waters extending as far as 150 miles.

The evidences of these offshore plumes, together with the one shown by Neshyba and Fonseca (1980), suggest that these patterns are a semipermanent feature within the area. This could be a part of the possible explanation of the migration regime of Jurel. Much more work must be done to demonstrate the biological and physical connections between the nearshore population and those which are currently being fished beyond the 200 miles EEZ.

Another example is related to the salmon project which is being carried out in southern Chile and around the Chiloe zone. As far as is known, the return of adult species has not been as successful as was expected. The problem here is also related to the knowledge of migration regimes of the species and of the physical circulation of the coastal ocean into which the juvenile

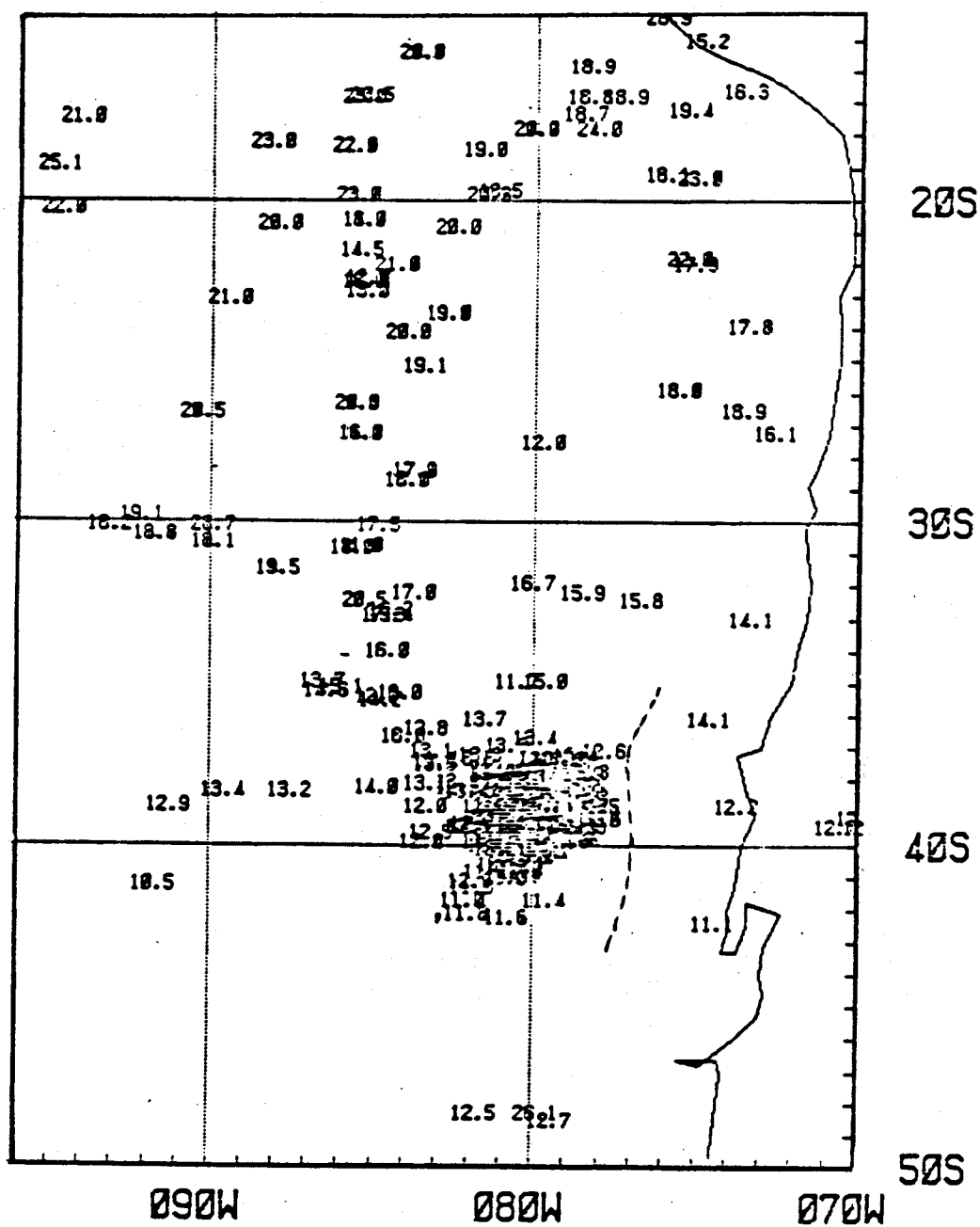


FIGURE 16. Chart of sea-surface temperature data off the coast of Chile. It shows the density of the data concentrated along 40°S and 200 miles offshore, which reflects the concentration of fishing boats catching Jurel, Jack Mackerel (*Trachurus murphyi*).

chum are introduced.

Finally, there are two or more important species in northern Chile which have suffered the consequences of the 1983 El Niño. Part of these populations could be migrating to waters with better conditions for their habitats. Subsequent changes in the biological activity also could be detected with the use of these chlorophyll images as well.

I believe that the link between ocean color and phytoplankton concentration afforded by the NIMBUS-7 CZCS offers an important and exciting new observational tool, not only for biologists and physicists, but also for fishery investigators.

BIBLIOGRAPHY

- Aldunate, Reinaldo H. and Hellmuth C. Sievers. 1977. Comparicion de temperaturas superficiales del mar obtenidas por sensores remotos y observaciones desde buques (septiembre y noviembre de 1975). *Cienc. y Tec. del mar, CONA No. 3.*
- Alhstrom, E. H. and O. P. Ball. 1954. Description of eggs and larvae of Jack mackerel (Trachurus symmetricus) and distribution and abundance of larvae in 1950-1951. *U.S. Fish, Wild. Serv. Fish. Bull. 56:209-245.*
- Baker, Karen S. and Raymond C. Smith. 1982. Bio-optical classification and model of natural waters. *Limnol. Oceanogr.*, 27(3): 500-509.
- Basten, J. 1978. Oceanografia de las aguas costeras del norte de Chile. Resultados del crucero de otoño de 1975 (May0). *Rev. Com. Perm. Pacifico Sur. 9:83-102.*
- Breaker, L. S. and R. P. Gilliland. 1980. A satellite sequence on upwelling along the California coast. *Coastal and Estuary Science 1, Coastal Upwelling Research, pp. 87-94.*
- Brooks, David A. and Richard V. Legeckis. 1982. A Ship and Satellite View of Hydrographic Feature in the Western Gulf of Mexico. *J. Geophys. Res. 87(C6):4195-4206.*
- Csanady, G. T. 1978. Wind Effects on Surface to Bottom Fronts. *J. Geophys. Res. 82(C9).*
- Enfield, David B. and J. S. Allen. 1980. On the Structure and Dynamics of Monthly Mean Sea Level Anomalies along the Pacific Coast of North and South America. *J. Phys. Oceanogr., Vol. 10:4.*
- Enfield, David B. 1981. Annual Nonseasonal Variability of Monthly Low-level Wind Fields over the Southeastern Tropical Pacific. *Mon. Wea. Rev. 109(10):2178-2190.*
- Espinoza, Felix R., Steve Neshyba and Zhao Maoxiang. 1983. Surface Water Motion Off Chile Revealed in Satellite Images of Surface Chlorophyll and Temperature. *Proceedings of the International Conference on Marine Resources of the Pacific, Viña del Mar, Chile.*
- Gordon, Howard R., Dennis K. Clark, James W. Brown, Otis B. Brown, Robert H. Evans and Williams W. Broenkow. 1983. Phytoplankton pigment concentrations in the Middle Atlantic Bight: comparison of ship determinations and CZCS estimates. *Applied Optics, 22:20-36.*

- Hovis, W. A., D. A. Clark, F. Anderson, R. W. Austin, W. H. Wilson, E. T. Baker, D. Ball, H. R. Gordon, J. L. Mueller, S. Z. El-Sayed, B. Sturm, R. C. Wrigler and C. S. Yentsch. 1980. Nimbus-7 Coastal Zone Color Scanner: System Description and Initial Imagery. *Science*, 210:60-63.
- Huh, Oscar K., Williams J. Wiseman, Jr., and Lawrence J. Rouse, Jr. 1978. Winter Cycle of Sea Surface Thermal Patterns, North-eastern Gulf of Mexico. *J. Geophys. Res.* 83(C9).
- Inostroza, J. 1972. Atlas Oceanografico de Chile. I.H.A. Pub. Inst. Hidro. de la Armada, Chile.
- _____. 1973. Some Oceanographic features of northern Chilean waters in July 1962. In: *Oceanography of the South Pacific*. Comp. R. Fraser. New Zealand National Commission for UNESCO, Wellington:37-46.
- Kao, Timothy W., Hsien-Ping Pao and Cheol Park. 1978. Surface Intrusions, Fronts, and Internal Waves: A Numerical Study. *J. Geophys. R.* 83(C9).
- Leetmaa, A. and Arthur D. Voorhis. 1978. Scales of Motion in the Subtropical Convergence Zone. *J. Geophys. Res.* 83(C9).
- Legeckis, Richard. 1978. A survey of Worldwide Sea Surface Temperature Fronts Detected by Environmental Satellites. *J. Geophys. Res.* 83(C9).
- Neshyba, Steve and Ricardo Z. Mendez. 1976. Analisis de temperaturas superficiales del mar como indicadores de movimientos de agua superficiales en el Pacifico Sr-Este. *Rev. Com. Perm. Pacifico Sur.* 5:129-137.
- Neshyba, Steve and Tomas R. Fonseca. 1980. Evidence for Counterflow to the West Wind Drift off South America. *J. Geophys. Res.* 85(C9):4888-4892.
- Pingree, R. D. and D. K. Griffiths. 1978. Tidal Fronts on the Shelf Seas around the British Isles. *J. Geophys. Res.* 83(C9).
- Quinn, William H. and Victor T. Neal. 1983. Southern Oscillation-related Climatic Changes and the 1982-1983 El Niño. Proceedings of the International Conference on Marine Resources of the Pacific, May 16-20, 1983, Viña del Mar, Chile.
- Robles, F. 1966. Descripcion grafica de las condiciones Oceanograficas frente a la provincia de Tarapaca en base a los datos de la Operacion Oceanografica MARCHILE II. I.H.A. Valpo, Chile.

- Robles, F., E. Alarcon and A. Ulloa. 1974. Water masses at the Northern Chilean zone and their variations in a cold period (1967) and warm period (1969, 1971-1973). Presented at Reunion de Trabajo sobre el Fenomeno El Niño. Auspiciado por la Comision Oceanografica Interyubernamental. Guayaquil, Ecuador.
- Sandoval, Eliseo T. 1971. The Summer Distribution of Tuna in Relation to the General Oceanographic Conditions off Chile and Peru. Bull. Far Seas Fish. Res. Lab., 5:23-88.
- Sievers, Hellmuth A. and Nelson Silva Sandoval. 1975. Masas de Agua y Circulacion en el Oceano Pacifico Sudoriental. Latitudes 18°S-33°S. Cienc. y Tec. del Mar. Contrib. CONA, 1: 7-67.
- Silva, Nelson S. and Steve Neshyba. 1977. Corrientes Superficiales frents a la Costa Austral de Chile. Cienc. y Tec. del Mar. CONA, 3:37-42.
- Silva, Nelson S. and Steve Neshyba. 1979. On the Southermost of the Peru-Chile Undercurrent. Deep-Sea Res., 26A:1387-1393.
- Silva, Nelson S. and Steve Neshyba. 1979/80. Masas de agua y circulacion geostrofica frente a la costa de Chile Austral. Ser. Cient. Inst. Antart. Chileno (25/26),5:32.
- Silva, Nelson S. and Hellmuth A. Sievers. 1981. Masas de Agua y Circulacion en la Region de la Rama Costera de la Corriente de Humboldt Latitudes 18°S-33°S. Cienc. y Tec. del Mar, CONA 5:5-50.
- Simpson, J. N., C. M. Allen and N. C. Morris. 1978. Fronts on the Continental Shelf. J. Geophys. Res., 83(C9).
- Smith, L. Robert. 1983. Circulation Patterns in Upwelling Regimes. Coastal Upwelling, Pt. A. Edited by Erwin Suess and Jorn Thied (Plenum Publishing Corporation).
- Smith, R. C. and K. S. Baker. 1982. Oceanic Chlorophyll Concentrations as Determined by Satellite (Nimbus-7 Coastal Zone Color Scanner). Marine Biology 66:269-279.
- Smith, R. C., R. W. Eppley and K. S. Baker. 1982. Correlation of Primary Production as Measured Aboard Ship in Southern California Coastal Waters and as Estimated from Satellite Chlorophyll Images. Marine Biology 66:281-288.
- Stumpf, Harry G. and Richard V. Legeckis. 1977. Satellite Observations of Mesoscale Eddy Dynamics in the Eastern Tropical Pacific Ocean. J. Phys. Oceanogr., 7:648-658.

Uribe, Eduardo, Steve Neshyba and Tomas Fonseca. 1982. Phytoplankton community composition across the West Wind Drift off South America. *Deep-Sea Res.*, 29(10A):1229-1243.

Uribe, Eduardo and Steve Neshyba. 1983. Phytoplankton Pigments from the Nimbus-7 Coastal Zone Color Scanner: Coastal Waters of Chile from 18°S to 40°S. *Proceedings of the International Conference on Marine Resources of the Pacific, Viña del Mar, Chile.*

Wooster, W. S. and M. Gilmartin. 1960. The Peru-Chile Undercurrent. *Jour. Mar. Res.* 19(3):97-122.

Wyrtki, K. 1963. The horizontal and vertical field of motion in the Peru Current. *Bull. Scrips Inst. of Ocean.*, 9(4):313-346.

_____. 1965. Summary of the Physical Oceanography of the Eastern Pacific Ocean. *Inst. of Mar. Resources. University of California.*

_____. 1966. Oceanography of the Eastern Equatorial Pacific Ocean. *Oceanogr. Mar. Biol. Ann. Rev.* 4:33-68.

_____. 1977. Advection in the Peru Current as Observed by Satellite. *J. Geophys. Res.*, 82(27):3939-3943.

APPENDICES

APPENDIX A

Fortran Listing of Filter Subroutine Used
with the Coastal Wind Time Series

```
PROGRAM PAS3COL(INPUT,OUTPUT,TAPE1,TAPE2)
DIMENSION FMT(8),TITLE(8),DTG(500),X(500,20),XMN(500,20)
COMMON/BAD/XMISS,XLIMIT
REWIND 1
REWIND 2
DO 30 I=1,500
DTG(I)=0.0
DO 30 L=1,20
30 X(I,L)=XMN(I,L)=0.0
XLIMIT=XMISS=999.9
INC=3
PRINT *," # SERIES = ",
READ *,NS
PRINT *," (FORMAT)",
READ 99,FMT
WRITE 99,FMT
DO 10 I=1,500
READ(2,FMT) DTG(I),(X(I,L),L=1,NS)
99 FORMAT(8A10)
IF(EOF(2).NE.0) GO TO 20
10 CONTINUE
20 N=I-1
DO 50 L=1,NS
CALL RUNMEAN(X(I,L),N,INC,XMN(I,L))
XMN(I,L)=XMN(N,L)=XLIMIT
50 CONTINUE
DO 60 I=1,N
WRITE(1,FMT) DTG(I),(XMN(I,L),L=1,NS)
60 CONTINUE
STOP
END
```

```
SUBROUTINE RUNMEAN(Y,NOBS,INC,YMEAN)
COMMON/BAD/XMISS,XLIMIT
DIMENSION Y(1),YMEAN(1),SUM(1800)
XINC=INC
NN=NOBS-INC+1
INT=XINC/2.
DO 20 I=1,NN
II=I+INT
SUM(I)=0.
C FIND SUM OVER NUMBER OF INCREMENTS DESIRED
DO 10 M=1,INC
K=M+(I-1)
IF(Y(K).EQ.XMISS.OR.ABS(Y(K)).GE.XLIMIT)GO TO 15
SUM(I)=SUM(I)+Y(K)
10 CONTINUE
YMEAN(II)=SUM(I)/XINC
GO TO 20
15 YMEAN(II)=XLIMIT
20 CONTINUE
RETURN
END
EOI ENCOUNTERED.
```

Appendix B

Fortran Listing of Plot Subroutine Used to
Make the Wind Stick Diagrams

CTSPLOTS

```

PROGRAM TSPLOTS(INPUT,OUTPUT,TAPE1,TAPE2,TAPE3,TAPE4
1,TAPE5,TAPE6,TAPE7,TAPE8,TAPE9,TAPE10,TAPE11
2,TAPE12,TAPE13,TAPE14)
DIMENSION NNN(9),IN(17),SUM(9),SSQ(9),IDTR(9),FMT(8),COEF(9)
DIMENSION NC(9)
COMMON /IO/ IWRT1,IWRT2
COMMON/PLT/ICODE,WIDTH,HEIGHT,NCHAR,LABELS(8),MODEL,IRATE,LUN
COMMON MO(1500),X(1500),Y(9,1500),YLIMIT,PLTGAP,YLO(9),YHI(9)
*,LBL(40.5),XSCALE,CSIZE,YLABEL,XTIC
DATA IWRT1 /14/
DATA IWRT2 /14/
REWIND 1
PRINT *," # SERIES,ICODE,MODEL,IRATE,YLIMIT,PLTGAP(IN)"
READ *,NSER,ICODE,MODEL,IRATE,YLIMIT,PLTGAP
PRINT *,"FORMAT (INCLUDE MONTH)",
READ 99,FMT
99 FORMAT(8A10)
PRINT *," DATA COLUMN = ",(L,L =1,NSER)
PRINT *," PLOT ORDER = ",
READ *,(NC(L),L=1,NSER)
DO 40 I=1,2100
READ(1,FMT) MO(I),(Y(NC(L),I),L=1,NSER)
IF(EOF(1).NE.0) GO TO 61
40 CONTINUE
61 LTS=I-1
PRINT *," FILE LENGTH= ",LTS
DO 66 L=1,NSER
YHI(L)=-YLIMIT
YLO(L)=YLIMIT
SUM(L)=SSQ(L)=0.0
66 NNN(L)=0
DO 65 I=1,LTS
DO 60 L=1,NSER
IF(Y(L,I).GE.YLIMIT) GO TO 60
YLO(L)=AMIN1(YLO(L),Y(L,I))
YHI(L)=AMAX1(YHI(L),Y(L,I))
NNN(L)=NNN(L)+1
SUM(L)=SUM(L)+Y(L,I)
SSQ(L)=SSQ(L)+Y(L,I)*Y(L,I)
60 CONTINUE
65 CONTINUE
DO 50 L=1,NSER
SUM(L)=SUM(L)/NNN(L)
SSQ(L)=SQRT((SSQ(L)-NNN(L)*SUM(L)*SUM(L))/(NNN(L)-1))

```



```

50 CONTINUE
  PRINT 96," # PTS= ",(NNN(L),L=1,NSER)
  PRINT 97," MEANS= ",(SUM(L),L=1,NSER)
  PRINT 97," STD'S= ",(SSQ(L),L=1,NSER)
  PRINT 97," MIN'S= ",(YLO(L),L=1,NSER)
  PRINT 97," MAX'S= ",(YHI(L),L=1,NSER)
96 FORMAT(A8,10I7)
97 FORMAT(A8,10F7.2)
98 FORMAT(/)
  PRINT *," ENTER AMPLIFICATION FACTORS: 1, 2, 3,...,ETC"
  READ *,(COEF(L),L=1,NSER)
  DO 502 L=1,NSER
  IF(COEF(L).GT.0.) GO TO 402
  YLO(L)=YHI(L)
  YHI(L)=YLO(L)
402 YLO(L)=YLO(L)*COEF(L)
  YHI(L)=YHI(L)*COEF(L)
502 CONTINUE
  DO 501 I=1,LTS
  DO 503 L=1,NSER
  IF(Y(L,I).NE.YLIMIT) Y(L,I)=Y(L,I)*COEF(L)
503 CONTINUE
  X(I)=I
501 CONTINUE
  CALL TSPLTS(LTS,NSER)
  STOP
  END

SUBROUTINE TSPLTS(N,LUNLIM)
  DIMENSION YSC(9),YDR(9),YTIC(9),NSMTICY(9),IVC(10),YSEP(9)
  COMMON/PLT/ICODE,WIDTH,HEIGHT,NCHAR,LABELS(8),MODEL,IRATE,LUN
  COMMON MO(1500),X(1500),Y(9,1500),YLIMIT,PLTGAP,YLO(9),YHI(9)
  *,LBL(40,5),XSCALE,Csize,YLABEL,XTIC
  PRINT *," XSCALE,X-AXIS,XTIC,NSMTICX,YLABEL,Csize"
  READ *,XSCALE,NORG,XTIC,NSMTICX,YLABEL,Csize
  PRINT *," YSCALE: 1, 2, 3,....., ETC.",
  READ *,(YSC(L),L=1,LUNLIM)
  PRINT *," YTIC: 1, 2, 3,....., ETC.",
  READ *,(YTIC(L),L=1,LUNLIM)
  PRINT *," NSMTICY: 1, 2, 3,....., ETC.",
  READ *,(NSMTICY(L),L=1,LUNLIM)
  PRINT *," ENTER =0 FOR X-AXIS AT Y=0; =1 FOR Y=YMIN: 1, 2,...,ETC"
  READ *,(YDR(L),L=1,LUNLIM)
  PRINT *," ENTER 0 FOR SCALAR, 1 FOR VECTOR COMP.: 1, 2, ...ETC"
  READ *,(IVC(L),L=1,LUNLIM)
  IF(MO(1).LE.12) GO TO 4
  PRINT *," INTERVAL FOR YEAR LABEL",

```

```

READ *,YI
4 IF(PLTGAP.NE.0.) GO TO 5
PRINT *," YSEP'S(UUNITS): 1, 2, 3,....., ETC.",
READ *,(YSEP(L),L=1,LUNLIM)
5 XLO=XORG=ITYPE=0.0
XBIAS=2.5
XHI=N
RANGE=0.0
DO 60 L=1,LUNLIM
PRINT *," NAME ",L," [50H]:",
READ 30,(LBL(L,K),K=1,5)
IF(YLABEL.LE.0.0) GO TO 31
PRINT *," Y-AXIS LABEL [50H]:"
READ 30,(LBL(L+LUNLIM,K),K=1,5)
30 FORMAT(5A10)
31 MNY=YLO(L)/YTIC(L)
IF(YLO(L).LT.0.0) MNY=MNY-1
MXY=YHI(L)/YTIC(L)
MXY=MXY+1
YLO(L)=MNY*YTIC(L)
YHI(L)=MXY*YTIC(L)
IF(YOR(L).NE.0) YOR(L)=YLO(L)
RANGE=RANGE+(YHI(L)-YLO(L))*YSC(L)
60 CONTINUE
IF(YLABEL.GE.0.0) GO TO 57
PRINT *," Y-AXIS LABEL [50H]:"
READ 30,(LBL(LUNLIM+LUNLIM,K),K=1,5)
57 WIDTH=XSCALE*N+5.
DYBIAS=YSC(1)*YTIC(1)/(NSMTICY(1)+1)
GAPS=PLTGAP*(LUNLIM-1)
IF(PLTGAP.NE.0.) GO TO 56
HH=0.
DO 55 L=1,LUNLIM
55 HH=HH+YSEP(L)*YSC(L)
HEIGHT=HH+YHI(1)*YSC(1)-YLO(LUNLIM)*YSC(LUNLIM)
*+2.*DYBIAS+2.
GO TO 58
56 IF(PLTGAP.GE.0.0) HEIGHT=GAPS+RANGE+2.5
IF(PLTGAP.LT.0.0) HEIGHT=-GAPS+YHI(1)*YSC(1)-
*YLO(LUNLIM)*YSC(LUNLIM)+2.*DYBIAS+4.*CSIZE
58 YBIAS=HEIGHT-2.*CSIZE
CALL PLOTTYPE(ICODE)
CALL TKTYPE(MODEL)
CALL BAUD(IRATE)
CALL TEKPAUS
CALL ERASE
CALL SIZE(WIDTH,HEIGHT)

```

```

CALL SCALE(XSCALE,0.1,XBIAS,YBIAS,0.0,0.0)
CALL AXIS(XLO,XHI,XLO,0.0,0.0,0.0,XTIC,0.0,NSMTICX,0)
CALL MOTICS(N,0.0,1.,YI)
YBIAS=YBIAS-DYBIAS-(YHI(1)-YLO(1))*YSC(1)
IGRIN=0
IVEC=0
XORG=XHI
DO 100 L=1,LUNLIM
IF(IVC(L).GT.0) IVEC=IVEC+1
IF(IVEC.LT.2) GO TO 40
IVEC=0
GO TO 100
40 LP1=L+1
DELY=YHI(L)-YLO(L)
IF(L.EQ.1) GO TO 300
IF(PLTGAP.GT.0.0) GO TO 295
LM1=L-1
IF(PLTGAP.EQ.0.) GO TO 294
YBIAS=YBIAS+YLO(L)*YSC(L)-YLO(LM1)*YSC(LM1)+PLTGAP
GO TO 300
294 YBIAS=YBIAS+YLO(L)*YSC(L)-YLO(LM1)*YSC(LM1)-YSEP(L)*YSC(L)
GO TO 300
295 YBIAS=YBIAS-PLTGAP-DELY*YSC(L)
300 CALL SCALE(XSCALE,YSC(L),XBIAS,YBIAS,XLO,YLO(L))
IF(NORG.GE.0) GO TO 65
IF(XORG.NE.XLO) GO TO 350
XORG=XHI
GO TO 65
350 XORG=XLO
65 CALL AXIS(XORG,XORG,XORG,YLO(L),YHI(L),YOR(L),XTIC,
YTIC(L),NSMTICX,NSMTICY(L))
C CALL MOTICS(N,YOR(L),0.,YI)
XWIDTH=CSIZE/XSCALE
YWIDTH=CSIZE/YSC(L)
IF(XORG.EQ.XLO) GO TO 120
XPOS=XHI-XWIDTH
GO TO 130
120 XPOS=-5.*XWIDTH
130 YY=YLO(L)
KLIM=DELY/YTIC(L)+1.
DO 70 K=1,KLIM
YPOS=YY-YWIDTH/2.
CALL NUMBER(XPOS,YPOS,0.0,CSIZE,-4,YY)
YY=YY+YTIC(L)
70 CONTINUE
IF(YLABEL.GT.0.0) CALL YLBL(XBIAS,LUNLIM,L)
YLAST=YLIMIT

```

```

      DO 80 I=1,N
      IPEN=1
      XI=X(I)
      YLI=Y(L,I)
      IF(IVC(L).EQ.0) GO TO 42
      CALL PLOT(XI,0.,0,MARK)
      XI=XI+Y(LP1,I)*YSC(LP1)/XSCALE
      YLI=Y(L,I)
      GO TO 44
42 IF(YLAST.EQ.YLIMIT) IPEN=0
44 IF(YLI.EQ.YLIMIT) IPEN=0
      CALL PLOT(XI,YLI,IPEN,MARK)
      YLAST=YLI
80 CONTINUE
C     XPTR=(XHI-XLO-30.*CSIZE/XSCALE)/2.
      XPTR=72.
C     YPTR=YLO(L) + CSIZE/YSC(L)
      YPTR=2.
      IF(IGRIN.NE.0) GO TO 101
      READ(8,*) XXX,YYY
      IF(EOF(8).EQ.0) GO TO 102
      IGRIN=1
101 CALL BELL
      CALL PLOT(XPTR,YPTR,0,0)
      CALL IGRINPT(XXX,YYY)
102 DO 75 K=1,5
      75 LABELS(K)=LBL(L,K)
      CALL SYMBOL(XXX,YYY,0.0,CSIZE,50,LABELS)
      WRITE(9,*) XXX,YYY
100 CONTINUE
      IF(YLABEL.LT.0.0) CALL YLBL(-.6*XBIAS/XSCALE,LUNLIM,
      *LUNLIM,IGRIN)
      IF(YLABEL.LT.0.0.AND.NORG.LT.0) CALL YLBL
      *((WIDTH-.5*XBIAS)/XSCALE,LUNLIM,LUNLIM,IGRIN)
      YBIAS=YBIAS-DYBIAS
      CALL SCALE(XSCALE,0.1,XBIAS,YBIAS,0.0,0.0)
      CALL AXIS(XLO,XHI,XLO,0.0,0.0,0.0,XTIC,0.0,NSMTICX,0)
      CALL MOTICS(N,0.0,-1.,YI)
      CALL PLOTEND
      RETURN
      END

      SUBROUTINE MOTICS(N,YOR,OPT,YI)
      COMMON MO(1500),X(1500),Y(9,1500),YLIMIT,PLTGAP,YLO(9),YHI(9)
      *,LBL(40,5),XSCALE,CSIZE,YLABEL,XTIC
      DIMENSION MON(12)
C ***** MONTH LABELS FOR 6-HRLY DATA

```

```

C   DATA MON/3RJAN,3HFEB,3HMAR,3HAPR,3HMAY,3HJUN,
C   *3HJUL,3HAUG,3HSEP,3HOCT,3HNOV,3HDEC/
C   **** MONTH LABELS FOR DAILY DATA
      DATA MON/1HJ,1HF,1HM,1HA,1HM,1HJ,1HJ,1HA,1HS,1HO,1HN,1HD/
      DY=0.66666*CSIZE
      XX=0.0
C   IF(MO(1).LE.12) DX=15.-.5*CSIZE/XSCALE
      IF(MO(1).LE.12) DX=60.-.5*CSIZE/XSCALE
      IF(MO(1).GT.12) DX=5.-CSIZE/XSCALE
      IF(OPT.LT.0.) DY=DY+CSIZE
      LAST=0
      DO 30 I=1,N
      IF(MO(I).EQ.LAST) GO TO 30
      IF(MO(I).GT.12) GO TO 10
      MCHAR=MON(MO(I))
10  IF(XTIC.NE.0.) GO TO 20
      CALL PLOT(X(I),YOR,0,0)
      CALL MARK(8)
      IF(MO(I).GT.12) GO TO 20
      CALL SYMBOL(X(I)+DX,DY*OPT*10.,0.,CSIZE,3,MCHAR)
      GO TO 25
20  MM=MO(I)/YI
      IY=YI
      MM=MM*IY
      IF(MM.EQ.MO(I)) ENCODE(10,99,MCHAR) MO(I)
99  FORMAT(I2)
15  IF(OPT.NE.0.AND.MM.EQ.MO(I)) CALL SYMBOL(X(I)+DX,DY*OPT*10.,
      *0.0,CSIZE,3,MCHAR)
25  LAST=MO(I)
30  CONTINUE
      RETURN
      END

      SUBROUTINE YLBL(XPOS,LUNLIM,L,IGRIN)
      COMMON/PLT/ICODE,WIDTH,HEIGHT,NCHAR,LABELS(8),MODEL,IRATE,LUN
      COMMON MO(1500),X(1500),Y(9,1500),YLIMIT,PLTGAP,YLO(9),YHI(9)
      *,LBL(40,5),XSCALE,CSIZE,YLABEL,XTIC
      IF(IGRIN.NE.0) GO TO 101
      READ(8,*) XXX,YYY
      IF(EOF(8).EQ.0) GO TO 102
101 YPOS=YHI(L)
      CALL PLOT(XPOS,YPOS,0,0)
      CALL BELL
      CALL IGRINPT(XXX,YYY)
102 DO 76 K=1,5
      76 LABELS(K)=LBL(LUNLIM+L,K)
      CALL SYMBOL(XXX,YYY,90.,CSIZE,50,LABELS)
      WRITE(9,*) XXX,YYY
      RETURN
      END

```

APPENDIX C

Meteorological Charts

Appendix C contains low-level cloud streams and wind vectors for the preceding six-day period of each of the chlorophyll mosaics analyzed in this paper. There are two meteorological charts per day for each of the periods.

From MM DD YY	Until MM DD YY
05 29 79	06 04 79
09 09 79	09 16 79
01 07 80	01 14 80
04 01 80	04 07 80

